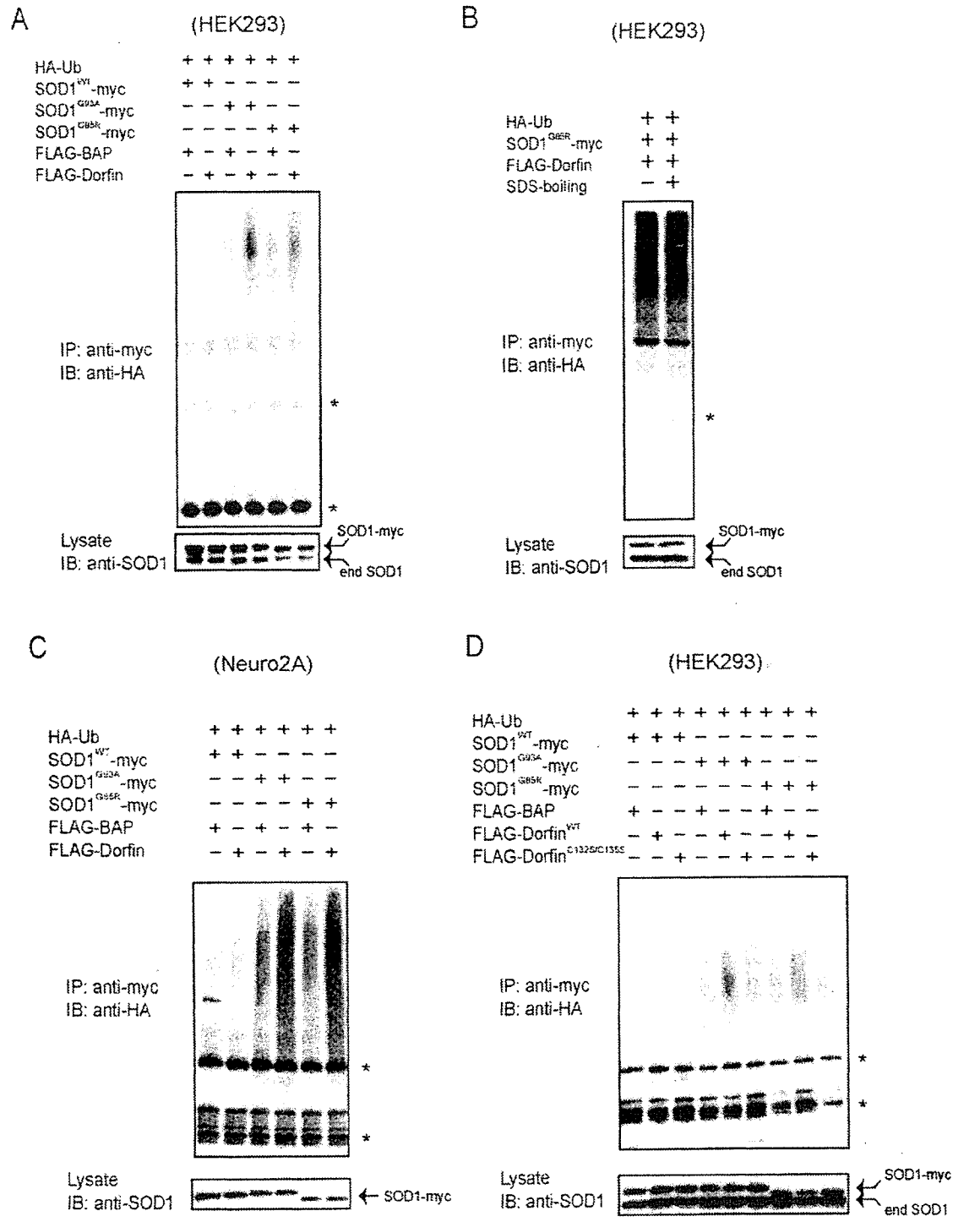

FIG. 6. **Dorfin ubiquitylates mutant SOD1s *in vivo*.** *A*, increased ubiquitylation of mutant SOD1 proteins by overexpression of Dorfin. HEK293 cells were co-transfected with $SOD1^{WT}$-Myc, $SOD1^{G93A}$-Myc, or $SOD1^{G85R}$-Myc and HA-Ub with or without FLAG-Dorfin. FLAG-bovine alkaline phosphatase (*BAP*) was used as a negative control. Immunoprecipitation (*IP*) was performed with Myc antibody (9E10). *IB*, immunoblotting. *B*, SDS boiling was performed prior to immunoprecipitation. To examine covalently ubiquitylated molecules, the cell lysate was boiled with the buffer containing 1% SDS for 5 min. Immunoprecipitation with Myc antibody (9E10) showed that the SDS-boiling procedure did not change polyubiquitylation level of $SOD1^{G85R}$-Myc by Dorfin. *C*, increased ubiquitylation of mutant SOD1 proteins by overexpression of Dorfin in Neuro2a cells. The same *in vivo* ubiquitylation assay as in *A* was performed using Neuro2a cells. *D*, $Dorfin^{C132S/C135S}$ ($Dorfin^{C132S/C135S}$) did not have E3 activity on mutant SOD1. HEK293 cells were co-transfected with $SOD1^{WT}$-Myc, $SOD1^{G93A}$-Myc, or $SOD1^{G85R}$-Myc and HA-Ub with FLAG-$Dorfin^{WT}$ or FLAG-$Dorfin^{C132S/C135S}$. The *asterisks* indicate IgG light and heavy chains.

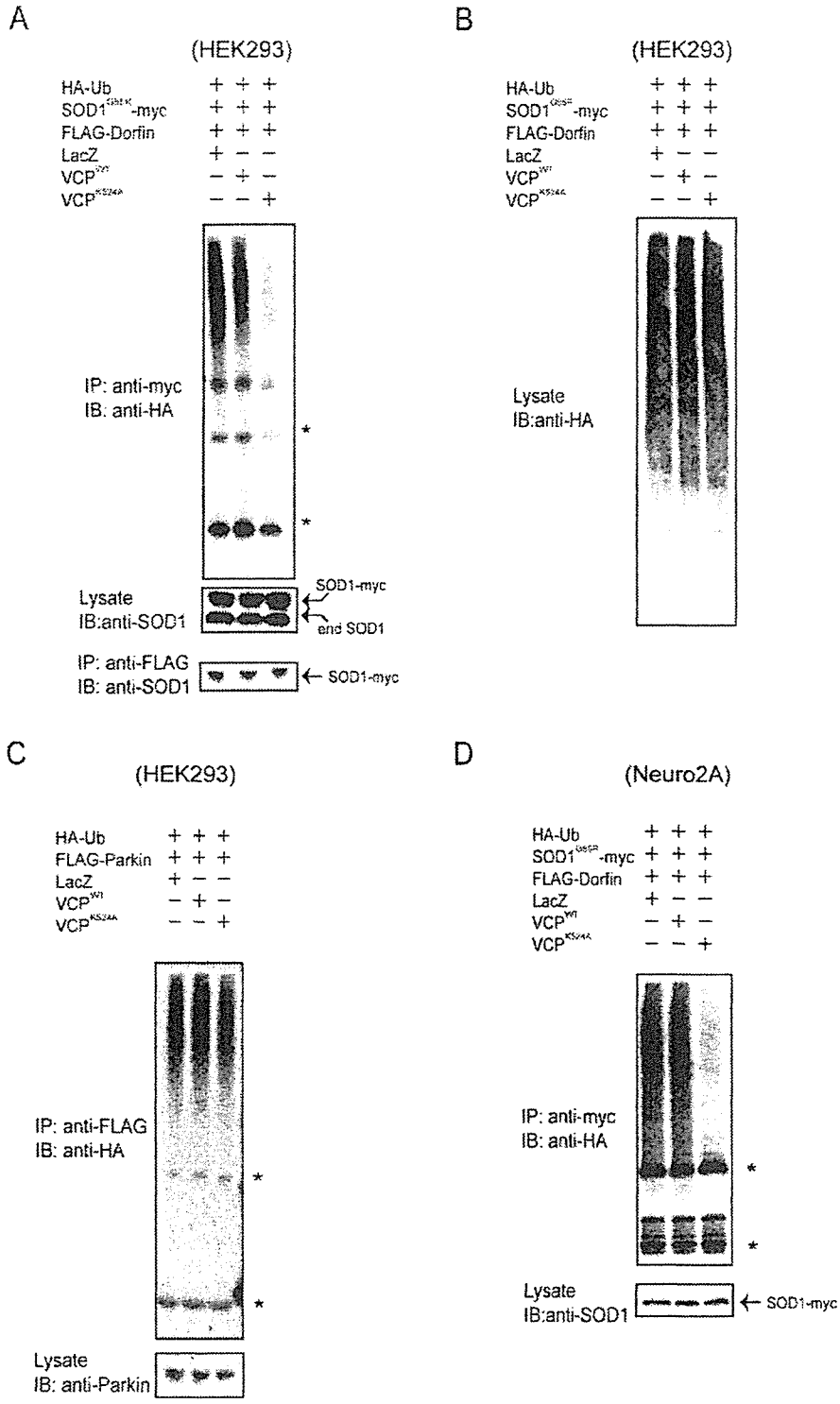

FIG. 7. **A dominant negative mutant of VCP, VCP^{K524A} inhibits the E3 ubiquitin ligase activity of Dorfin.** *A*, inhibition of dominant negative form mutant VCP^{K524A} on the E3 ubiquitin ligase activity of Dorfin. HEK293 cells were co-transfected with $SOD1^{G85R}$-Myc, HA-Ub, FLAG-Dorfin, and VCP^{WT}, VCP^{K524A}, or LacZ. Immunoprecipitation (*IP*) was performed with Myc antibody (9E10) and FLAG antibody (M2). *IB*, immunoblotting. *B*, neither VCP^{WT} nor VCP^{K524A} changed the level of total polyubiquitylated protein in the cell lysate. Ten percent of the volume of HEK293 cells used in *A* was subjected to immunoblotting using anti-HA (12CA5) antibody. *C*, autoubiquitylation of FLAG-Parkin was not influenced by the dominant negative form VCP^{K524A}. HEK293 cells were co-transfected with FLAG-Parkin, HA-Ub, and VCP^{WT}, VCP^{K524A}, or LacZ. Immunoprecipitation with FLAG antibody (M2) was performed. *D*, inhibition of VCP^{K524A} on E3 ubiquitin ligase activity of Dorfin in Neuro2a cells. Neuro2a cells were co-transfected with $SOD1^{G85R}$-Myc, HA-Ub, FLAG-Dorfin, and VCP^{WT}, VCP^{K524A}, or LacZ. Immunoprecipitation was performed using Myc antibody (9E10) and FLAG antibody (M2). The *asterisks* indicate IgG light and heavy chains.

The amount of Dorfin bound with VCP was saturated at even molar ratio *in vitro* (Fig. 3, *B* and *C*). Since VCP exists as a homohexamer (Fig. 3*D*), the *in vivo* observed size of ~600 kDa appears to be too small for the Dorfin-VCP complex if one VCP molecule binds to more than one Dorfin as shown in *in vitro* experiments. However, it is noteworthy that the size of molecules estimated by glycerol density gradient centrifugation analysis used in this study is not accurate and sufficient to discuss the molecular interaction of Dorfin and VCP in the cells. To date, various adaptor proteins, with which VCP forms multiprotein complexes, have been identified, such as Npl4, Ufd1 (18, 20), Ufd2 (34), Ufd3 (35), p47 (36), or SVIP (37). Although our *in vitro* study showed direct physical interaction between Dorfin and VCP, the environment with those adaptor proteins might reflect *in vivo* conditions. This also may explain the apparent discrepancy of the Dorfin-VCP binding fashions between *in vivo* and *in vitro* analyses.

Treatment with a proteasomal inhibitor causes the translocation of endogenous VCP and Dorfin to the aggresome in cultured cells (4, 15). Our results showed that these two proteins indeed colocalized perinuclearly in the aggresome following treatment with a proteasomal inhibitor (Fig. 4). Furthermore, we were able to demonstrate both Dorfin and VCP immunoreactivities in LB-like inclusions in ALS and LBs in PD (Fig. 5). In the majority of LBs, indistinguishable peripheral staining patterns were observed with both anti-Dorfin and anti-VCP antibodies. These results confirmed that both Dorfin and VCP are associated with the formation processes of aggresomes and inclusion bodies through physical interaction.

We showed here that co-expression of VCP^{K524A} resulted in a marked decrease of ubiquitylation activity of Dorfin compared with co-expression of VCP^{WT} or control. On the other hand, VCP^{K524A} failed to decrease autoubiquitylation activity of Parkin. VCP^{K524A} did not change the level of polyubiquitylated protein accumulation in the cell lysate in this study (Fig. 7). Knockdown experiments using the RNA interference technique showed accumulation of polyubiquitylated proteins (38). Combined with the observation that inhibition of VCP did not decrease the general accumulation of polyubiquitylated proteins, our results indicated that the E3 regulation function of VCP may be specific to certain E3 ubiquitin ligases such as Dorfin. VCP is an abundant protein that accounts for more than 1% of protein in the cell cytosol and is known to have various chaperone-like activities (39); therefore, it may function as a scaffold protein on the E3 activity of Dorfin. The localization of Dorfin and VCP in UBIs in various neurodegenerative disorders indicates the involvement of these proteins in the quality control system for abnormal proteins accumulated in the affected neurons in neurodegenerative disorders.

Since the unfolded protein response and ERAD are dynamic responses required for the coordinated disposal of misfolded proteins (40), the ERAD pathway can be critical for the etiology of neuronal cell death caused by various unfolded proteins. VCP is required for multiple aspects of the ERAD system by recognition of polyubiquitylated proteins and translocations to the 26 S proteasome for processive degradation through the VCP-Npl4-Ufd1 complex (18, 41). Our results suggest the involvement of Dorfin in the ERAD system, which is related to the pathogenesis of neurodegenerative disorders, such as PD or Alzheimer's disease. Further study including Dorfin knockout and/or knockdown models should examine the pathophysiology of Dorfin in association with the ERAD pathway or other cellular functions. Such studies should enhance our understanding of the pathogenetic role of Dorfin in neurodegenerative disorders.

REFERENCES

1. Julien, J. P. (2001) *Cell* **104,** 581–591
2. Rowland, L. P., and Shneider, N. A. (2001) *N. Engl. J. Med.* **344,** 1688–1700
3. Ishigaki, S., Niwa, J., Ando, Y., Yoshihara, T., Sawada, K., Doyu, M., Yamamoto, M., Kato, K., Yotsumoto, Y., and Sobue, G. (2002) *FEBS Lett.* **531,** 354–358
4. Niwa, J., Ishigaki, S., Doyu, M., Suzuki, T., Tanaka, K., and Sobue, G. (2001) *Biochem. Biophys. Res. Commun.* **281,** 706–713
5. Niwa, J., Ishigaki, S., Hishikawa, N., Yamamoto, M., Doyu, M., Murata, S., Tanaka, K., Taniguchi, N., and Sobue, G. (2002) *J. Biol. Chem.* **277,** 36793–36798
6. Ciechanover, A., and Brundin, P. (2003) *Neuron* **40,** 427–446
7. Hishikawa, N., Niwa, J., Doyu, M., Ito, T., Ishigaki, S., Hashizume, Y., and Sobue, G. (2003) *Am. J. Pathol.* **163,** 609–619
8. Mayer, R. J., Lowe, J., Lennox, G., Doherty, F., and Landon, M. (1989) *Prog. Clin. Biol. Res.* **317,** 809–818
9. Johnston, J. A., Ward, C. L., and Kopito, R. R. (1998) *J. Cell Biol.* **143,** 1883–1898
10. Kopito, R. R. (2000) *Trends Cell Biol.* **10,** 524–530
11. Kobayashi, T., Tanaka, K., Inoue, K., and Kakizuka, A. (2002) *J. Biol. Chem.* **277,** 47358–47365
12. Shimura, H., Hattori, N., Kubo, S., Mizuno, Y., Asakawa, S., Minoshima, S., Shimizu, N., Iwai, K., Chiba, T., Tanaka, K., and Suzuki, T. (2000) *Nat. Genet.* **25,** 302–305
13. Fukuchi, M., Imamura, T., Chiba, T., Ebisawa, T., Kawabata, M., Tanaka, K., and Miyazono, K. (2001) *Mol. Biol. Cell* **12,** 1431–1443
14. Ishigaki, S., Liang, Y., Yamamoto, M., Niwa, J., Ando, Y., Yoshihara, T., Takeuchi, H., Doyu, M., and Sobue, G. (2002) *J. Neurochem.* **82,** 576–584
15. Hirabayashi, M., Inoue, K., Tanaka, K., Nakadate, K., Ohsawa, Y., Kamei, Y., Popiel, A. H., Sinohara, A., Iwamatsu, A., Kimura, Y., Uchiyama, Y., Hori, S., and Kakizuka, A. (2001) *Cell Death Differ.* **8,** 977–984
16. Natsume, T., Yamauchi, Y., Nakayama, H., Shinkawa, T., Yanagida, M., Takahashi, N., and Isobe, T. (2002) *Anal. Chem.* **74,** 4725–4733
17. Matsuda, N., Suzuki, T., Tanaka, K., and Nakano, A. (2001) *J. Cell Sci.* **114,** 1949–1957
18. Bays, N. W., and Hampton, R. Y. (2002) *Curr. Biol.* **12,** R366–R371
19. Ye, Y., Meyer, H. H., and Rapoport, T. A. (2001) *Nature* **414,** 652–656
20. Braun, S., Matuschewski, K., Rape, M., Thoms, S., and Jentsch, S. (2002) *EMBO J.* **21,** 615–621
21. Jarosch, E., Taxis, C., Volkwein, C., Bordallo, J., Finley, D., Wolf, D. H., and Sommer, T. (2002) *Nat. Cell Biol.* **4,** 134–139
22. Rabinovich, E., Kerem, A., Frohlich, K. U., Diamant, N., and Bar-Nun, S. (2002) *Mol. Cell. Biol.* **22,** 626–634
23. Mizuno, Y., Hori, S., Kakizuka, A., and Okamoto, K. (2003) *Neurosci. Lett.* **343,** 77–80
24. Ito, T., Niwa, J., Hishikawa, N., Ishigaki, S., Doyu, M., and Sobue, G. (2003) *J. Biol. Chem.* **278,** 29106–29114
25. Meyer, H. H., Kondo, H., and Warren, G. (1998) *FEBS Lett.* **437,** 255–257
26. Kondo, H., Rabouille, C., Newman, R., Levine, T. P., Pappin, D., Freemont, P., and Warren, G. (1997) *Nature* **388,** 75–78
27. Rabouille, C., Kondo, H., Newman, R., Hui, N., Freemont, P., and Warren, G. (1998) *Cell* **92,** 603–610
28. Hetzer, M., Meyer, H. H., Walther, T. C., Bilbao-Cortes, D., Warren, G., and Mattaj, I. W. (2001) *Nat. Cell Biol.* **3,** 1086–1091
29. Frohlich, K. U., Fries, H. W., Rudiger, M., Erdmann, R., Botstein, D., and Mecke, D. (1991) *J. Cell Biol.* **114,** 443–453
30. Asai, T., Tomita, Y., Nakatsuka, S., Hoshida, Y., Myoui, A., Yoshikawa, H., and Aozasa, K. (2002) *Jpn. J. Cancer Res.* **93,** 296–304
31. Kawaguchi, Y., Okamoto, T., Taniwaki, M., Aizawa, M., Inoue, M., Katayama, S., Kawakami, H., Nakamura, S., Nishimura, M., Akiguchi, I., Kimura, J., Narumiya, S., and Kakizuka, A. (1994) *Nat. Genet.* **8,** 221–228
32. Matsumoto, M., Yada, M., Hatakeyama, S., Ishimoto, H., Tanimura, T., Tsuji, S., Kakizuka, A., Kitagawa, M., and Nakayama, K. I. (2004) *EMBO J.* **23,** 659–669
33. Watts, G. D., Wymer, J., Kovach, M. J., Mehta, S. G., Mumm, S., Darvish, D., Pestronk, A., Whyte, M. P., and Kimonis, V. E. (2004) *Nat. Genet.* **36,** 377–381
34. Koegl, M., Hoppe, T., Schlenker, S., Ulrich, H. D., Mayer, T. U., and Jentsch, S. (1999) *Cell* **96,** 635–644
35. Ghislain, M., Dohmen, R. J., Levy, F., and Varshavsky, A. (1996) *EMBO J.* **15,** 4884–4899
36. Meyer, H. H., Wang, Y., and Warren, G. (2002) *EMBO J.* **21,** 5645–5652
37. Nagahama, M., Suzuki, M., Hamada, Y., Hatsuzawa, K., Tani, K., Yamamoto, A., and Tagaya, M. (2003) *Mol. Biol. Cell* **14,** 262–273
38. Wojcik, C., Yano, M., and DeMartino, G. N. (2004) *J. Cell Sci.* **117,** 281–292
39. Dalal, S., and Hanson, P. I. (2001) *Cell* **104,** 5–8
40. Travers, K. J., Patil, C. K., Wodicka, L., Lockhart, D. J., Weissman, J. S., and Walter, P. (2000) *Cell* **101,** 249–258
41. Dai, R. M., and Li, C. C. (2001) *Nat. Cell Biol.* **3,** 740–744

THE JOURNAL OF BIOLOGICAL CHEMISTRY
Vol. 279, No. 51, Issue of December 17, pp. 53427–53434, 2004
Printed in U.S.A.

An RNA-interacting Protein, SYNCRIP (Heterogeneous Nuclear Ribonuclear Protein Q1/NSAP1) Is a Component of mRNA Granule Transported with Inositol 1,4,5-Trisphosphate Receptor Type 1 mRNA in Neuronal Dendrites*[S]

Received for publication, August 24, 2004, and in revised form, October 5, 2004
Published, JBC Papers in Press, October 8, 2004, DOI 10.1074/jbc.M409732200

Hiroko Bannai‡§, Kazumi Fukatsu§, Akihiro Mizutani‡¶, Tohru Natsume‖, Shun-ichiro Iemura‖, Tohru Ikegami§, Takafumi Inoue§¶, and Katsuhiko Mikoshiba‡§¶‡‡**

From the ‡Laboratory for Developmental Neurobiology, Brain Science Institute, RIKEN, 2-1 Hirosawa, Wako, Saitama 351-0198, Japan, §Division of Molecular Neurobiology and ‡‡Division of Neural Signal Information NTT-IMSUT, The Institute of Medical Science, The University of Tokyo, 4-6-1 Shirokanedai, Minato-ku, Tokyo 108-8639 Japan, ¶Calcium Oscillation Project, ICORP, Japan Science and Technology Corp., 3-4-4 Shirokanedai, Minato-ku, Tokyo 108-0071, Japan, and ‖National Institute of Advanced Industrial Science and Technology, Biological Information Research Center, 2-41-6 Ohmi, Kohtoh-ku, Tokyo 135-0064, Japan

mRNA transport and local translation in the neuronal dendrite is implicated in the induction of synaptic plasticity. Recently, we cloned an RNA-interacting protein, SYNCRIP (heterogeneous nuclear ribonuclear protein Q1/NSAP1), that is suggested to be important for the stabilization of mRNA. We report here that SYNCRIP is a component of mRNA granules in rat hippocampal neurons. SYNCRIP was mainly found at cell bodies, but punctate expression patterns in the proximal dendrite were also seen. Time-lapse analysis in living neurons revealed that the granules labeled with fluorescent protein-tagged SYNCRIP were transported bi-directionally within the dendrite at ~0.05 μm/s. Treatment of neurons with nocodazole significantly inhibited the movement of green fluorescent protein-SYNCRIP-positive granules, indicating that the transport of SYNCRIP-containing granules is dependent on microtubules. The distribution of SYNCRIP-containing granules overlapped with that of dendritic RNAs and elongation factor 1α. SYNCRIP was also found to be co-transported with green fluorescent protein-tagged human staufen1 and the 3′-untranslated region of inositol 1,4,5-trisphosphate receptor type 1 mRNA. These results suggest that SYNCRIP is transported within the dendrite as a component of mRNA granules and raise the possibility that mRNA turnover in mRNA granules and the regulation of local protein synthesis in neuronal dendrites may involve SYNCRIP.

Protein synthesis in neurons was long believed to occur only in the cell body, but recent evidence showing the presence of mRNA (for review, see Refs. 1–4) and the capacity for local translation of specific mRNAs in neuronal dendrites (Refs. 5 and 6; for review, see Refs. 7 and 8) has changed this belief. Selective transport and localization of certain types of mRNA and subsequent local protein synthesis in neuronal dendrites are now considered as part of the fundamental mechanisms involved in synaptic plasticity.

Various kinds of mRNA, such as mRNA-coding cytoskeletal proteins (MAP2, β-actin, Arc (activity-regulated cytoskeleton-associated protein), and neurofilament proteins), kinases (*e.g.* the α subunit of Ca^{2+}/CaM[1] kinase II (CaMKIIα)), receptors and channels (glycine receptors, glutamate receptors, and inositol 1,4,5-trisphosphate receptor type 1 (IP_3R1)) have been reported to target dendrites of central nervous system neurons (for review, see Refs.4, 8). Many of the mRNAs listed above are transported to the dendrites as a component of ribonucleoprotein complexes called mRNA granules, which were detected with fluorescent dye SYTO14 (9) and by the *in situ* hybridization technique (10, 11). mRNA granules contain ribosomes and other components of translational machinery (9, 12, 13) as well as various mRNA-binding proteins, including fragile X mental retardation protein (14), staufen (15), testis-brain RNA-binding protein (16), zip code-binding protein 1 (17), and heterogeneous nuclear ribonuclear protein (hnRNP) A2 (18). These mRNA-binding proteins are thought to be responsible for the stability and the translational regulation of mRNAs; however, their actual function in dendrites is poorly understood.

We recently discovered a novel RNA-interacting protein, SYNCRIP (synaptotagmin binding, cytoplasmic RNA-interacting protein (19)) in mouse. A human homolog of SYNCRIP was termed as NSAP1 (20) or hnRNP Q1 (21). SYNCRIP is one of three alternative splicing variants (21) and has high homology to hnRNP R. Interestingly, in contrast to hnRNP R and other splicing variants of SYNCRIP (hnRNP Q2 and Q3), SYNCRIP is distributed throughout the cytosol instead of being localized in the nucleus (19). SYNCRIP binds to RNA *in vitro*, preferen-

* This study was supported by grants from the Ministry of Education, Culture, Sports, Science, and Technology (MEXT) of Japan (to T. Inoue and K. M.), the Ministry of Health, Labor, and Welfare of Japan (to T. Inoue), and the 21st Century Center of Excellence Program, Center for Integrated Brain Medical Science from MEXT of Japan (to K. F.). The costs of publication of this article were defrayed in part by the payment of page charges. This article must therefore be hereby marked "*advertisement*" in accordance with 18 U.S.C. Section 1734 solely to indicate this fact.

[S] The on-line version of this article (available at http://www.jbc.org) contains supplemental Table SI, supplemental Data S1, and the legends for supplemental Movies 1–3.

** To whom correspondence should be addressed: Division of Molecular Neurobiology, The Institute of Medical Science, The University of Tokyo, 4-6-1 Shirokanedai, Minato-Ku, Tokyo, 108-8639, Japan. Tel.: 81-3-5449-5320; Fax: 81-3-5449-5420; E-mail: tinoue@ims.u-tokyo.ac.jp.

[1] The abbreviations used are: CaM, calmodulin; CaMKIIα, α subunit of Ca^{2+}/CaM kinase II; IP_3R1, inositol 1,4,5-trisphosphate receptor type 1; hnRNP, heterogeneous nuclear ribonuclear protein; SYNCRIP, synaptotagmin binding cytoplasmic RNA-interacting protein; PBS, phosphate-buffered saline; GFP, green fluorescent protein; mRFP, monomeric red fluorescent protein; NLS, nuclear localization signal; 3′-UTR, 3′-untranslated region; MS2bs, MS2 phage coat protein binding sequences; EF1α, elongation factor1α; EtBr, ethidium bromide; CCD, charge-coupled device; A2RE, hnRNP A2 response element.

tially to poly (A) or poly (U), in a phosphorylation-dependent manner (19, 22, 23). Although SYNCRIP is reported to be a component of protein complexes that stabilize c-*fos* proto-oncogene mRNA in mammalian culture cells (24), the physiological role of SYNCRIP in the cytoplasm is not yet understood. In this study we performed a proteomic analysis of the protein complexes that associate with SYNCRIP in human kidney cell line 293EBNA and found that SYNCRIP preferentially associated with ribosomal proteins and RNA-binding proteins. We also found that SYNCRIP is a component of mRNA granules containing IP_3R1 mRNA transported within the dendrites in a microtubule-dependent manner.

EXPERIMENTAL PROCEDURES

Proteomic Analysis—Proteomics analysis of the proteins that associate with SYNCRIP was performed as previously described (25–27). In brief, human 293EBNA cells were harvested, washed with phosphate-buffered saline (PBS), and lysed at 24 h after the transfection of cDNA coding FLAG-tagged SYNCRIP. Then the resulting cell lysate was incubated with M2-agarose overnight at 4 °C for immunoprecipitation. The protein-bound agarose beads were washed extensively, and the proteins were eluted with FLAG peptide. The isolated complex was precipitated using mixed methanol and chloroform. After vacuum-drying, the precipitate was digested with *Achromobacter* protease I. The digested peptide mixture were analyzed using a Direct nano flow LC-MSM system as described (26), and protein identification was performed according to the criteria described previously (26).

Construction of Fusion Proteins—FLAG-tagged SYNCRIP was generated by subcloning PCR-amplified DNA fragment coding mouse SYNCRIP (19) fused with FLAG tag to its N terminus into pcDNA3 (Invitrogen). To construct a green fluorescent protein (GFP)-tagged SYNCRIP, the coding sequence of mouse SYNCRIP was subcloned into the PstI/KpnI site of pEGFP-C3 (Clontech, Palo Alto, CA). Monomeric red fluorescent protein (mRFP)-tagged SYNCRIP (mRFP-SYNCRIP) was generated by fusing a mRFP, a gift from Dr. R. Tsien (28), to the N terminus of SYNCRIP with the amino acids Glu-Phe as a linker, which was then subcloned into pcDNA3.1/Zeo+ (Invitrogen). To construct GFP-fused human staufen1 (GFP-hStau1), the coding region of hStau1 was amplified from HEP22160 (a gift from Dr. S. Sugano) and subcloned into the XhoI/HindIII site of pEGFP-C1 (Clontech).

NLS-MS2-Venus was generated from pGA14-MS2-GFP (a gift from Dr. R. Singer (29)) and pCS2-Venus (a gift from Dr. A. Miyawaki). A coding sequence of "Venus" (a variant of yellow fluorescent protein (30)) was PCR-amplified with 5′-GTGCGGCCGCTGGTATGAGCAAGGGC-GAGG-3′and 5′-CTTGAATTCTTACTTGTACAG-3′ using pCS2-Venus as a template. The NotI-EcoRI digest of the resultant cDNA fragment and the BamHI-NotI digest of pG14-MS2-GFP that corresponded to the coding sequence of MS2 coat protein and nuclear localization signal (NLS) were then introduced into the BamHI/EcoRI site of a mammalian expression vector pCS2+.

To construct the RNA expression vector of the 3′-untranslated regions (3′-UTR) of IP_3R1 (IP_3R1 3′-UTR-MS2bs), we amplified a cDNA fragment of 3′-UTR of mouse IP_3R1 (bases 8579–9041) by PCR using primers 5′-GGCTCGAGGCAAATGAGGCAGAGGGAC-3′, and 5′-GCG-GGCCCAACCATTTATTACACGAGTATCAAC-3′. The resulting PCR fragment was subcloned into the XhoI/ApaI site of pcDNA3.1/Zeo+, upstream of which 12 copies of MS2 phage coat protein binding sequences (MS2bs) and the coding sequence of alkaline phosphatase were inserted, and the bovine growth hormone polyadenylation signal downstream to the multicloning site was removed.

Cell Culture and Transfection—Primary cultures of neurons were prepared from hippocampi of 1-day-old Wistar rats by a standard method as described previously (31, 32) and plated on poly-L-lysine (Nacalai Tesque, Kyoto, Japan)-coated coverslips at a density of 4.6×10^4-1.3×10^5 cells/cm^2. Cells were cultured in Neurobasal medium (Invitrogen) supplemented with 2.5 mM L-glutamine (Nacalai Tesque), 2.5% (v/v) B-27 (Invitrogen), and antibiotics (250 units/ml penicillin and 250 μg/ml streptomycin). The cultures were transfected with 10 μg of DNAs by a standard calcium phosphate method (33) or 2.5 μg of DNAs by lipofection using Lipofectamine 2000 (Invitrogen) (34) on days 5–6 *in vitro*. For the labeling of 3′-UTR of IP_3R1 mRNA, 0.6 μg of NLS-MS2-Venus and 1.8 μg of IP_3R1 3′-UTR-MS2bs were co-transfected by lipofection. The transfected cells were used for immunohistochemistry or imaging experiments 2–3 days after the transfection, which corresponded to days 7–9 *in vitro*.

Antibodies—The rabbit antibody recognizing the N-terminal region of SYNCRIP, anti-SYNCRIP-N antibody, was obtained as described previously (19). Anti-SYNCRIP-N was used after affinity purification, and the specificity of this antibody has been confirmed by parallel experiments using preimmune serum or anti-SYNCRIP-N antibody preincubated with an excess amount of antigenic polypeptide (19). Anti-elongation factor1α (EF1α) antibody was from Upstate Biotechnology (Charlottesville, VA, clone CBP-KK1). Alexa 488- or Alexa 594-conjugated secondary antibody was from Molecular Probes (Eugene, OR).

Immunohistochemistry, Cell Labeling Experiments, and Confocal Imaging—For immunohistochemistry of native hippocampus, Wistar rats were deeply anesthetized on postnatal day 7 and perfused with 4% paraformaldehyde in PBS. Whole brains were removed and post-fixed in the same fixative overnight at 4 °C. Sagittal sections (thickness, 100 μm) were cut with a Vibratome-type micro slicer (DTK-1500; Dosaka EM, Kyoto, Japan), collected in PBS, and permeabilized with 0.3% Triton X-100. After incubating with blocking solution (1% bovine serum albumin and 0.3% Triton X-100 in PBS) sections were incubated with anti-SYNCRIP-N antibody (1:1000 dilution) in blocking solution overnight at 4 °C and subsequently with Alexa 488-conjugated anti rabbit IgG (Molecular Probes) for 3 h at room temperature. Finally, sections were mounted on slides with Vectashield (Vector Laboratories, Burlingame, CA) and observed under a confocal-scanning microscope (FV-300; Olympus, Tokyo, Japan) attached to an inverted microscope (IX70; Olympus) with a ×10 objective (NA 0.30; Olympus) and a ×40 objective (NA 0.85; Olympus).

For immunostaining of cultured neurons, cells were fixed with 4% formaldehyde in PBS for 10 min. After permeabilization with 0.1% Triton X-100 in PBS for 10 min and blocking with 5% skim milk in PBS, the cells were incubated with the primary antibodies at 1:1000 dilution for anti-SYNCRIP-N antibody and at 1:400 dilution for anti-EF1α antibody. Alexa 488- or Alexa 594-conjugated IgGs (Molecular Probes) were used as secondary antibodies. RNA labeling with ethidium bromide (EtBr) was performed as described previously (35). RNase treatment was conducted by incubating neurons with 20 μg/ml RNase A (Nippongene, Tokyo, Japan) for 15 min after the EtBr staining. For labeling hippocampal neurons with endosomal and lysosomal markers, cells were incubated with 1 mg/ml Texas Red-dextran (M_r 3000; Molecular Probes) overnight. Fluorescence images of cultured neurons were taken under a confocal-scanning microscope (FV-300) using a 60× objective (NA 1.4; Olympus).

All of the images taken by the confocal microscope were digitally smoothed to reduce the noise level. The smoothing filter was implemented using 3 × 3 spatial convolutions, where the value of each pixel in the selection was replaced with the weighted average of its 3 × 3 neighborhood. Center pixels are 4-fold weighted over surrounding pixels.

Time-lapse Imaging and Data Analysis—The culture medium was supplemented with 20 mM HEPES (pH 7.3) for the time-lapse imaging experiments. The temperature was maintained at ~37 °C by a heating chamber that surrounded the microscope stage. For single color time-lapse imaging, the cells were visualized under an inverted microscope (IX70, Olympus) and a 60× objective (NA 1.45, Olympus) using standard filter sets and a mercury lamp. Sequential images were acquired with a cooled charge-coupled device (CCD) camera (ORCA-ER; Hamamatsu Photonics, Hamamatsu, Japan) with a 58- or 117-ms exposure time every 10 s. For multicolor time-lapse imaging, neurons were visualized under an inverted microscope (IX81; Olympus) equipped with a motorized fluorescence mirror unit exchanger, standard filter sets, and a 60× objective (NA 1.4; Olympus). Images were taken with a cooled CCD camera (ORCA-ER) with a 200-ms exposure time every 10 s.

Data were analyzed using TI Workbench, which is a custom-made software written by T. Inoue. Positions of fluorescent vesicles were plotted against time, and velocity of the granular movements was obtained by linear fitting of the slope. Only structures moving in more than three image frames were taken into account. The velocities were calculated for each period of consecutive movement. Images of time-lapse (Figs. 3*A*, 6*B*, and 7*C*) presented in this study were subjected to digital smoothing with the same algorithm as the confocal images (see above) to reduce the noise level.

Drug Preparation and Drug Treatment—Stock solutions of nocodazole (10 mg/ml, Sigma) and latrunculin A (1 mg/ml, Molecular Probes) were prepared in dimethyl sulfoxide (Me_2SO) and stored at −20 °C. Neurons were incubated with nocodazole (30 μg/ml) and latrunculin A (1 μg/ml) for 1 h at 37 °C in 5% CO_2. To confirm that the cytoskeleton was disrupted, fixed cells were stained with anti-tubulin antibody (Lab Vision, CA) or Alexa 594-phalloidin (Molecular Probes). We found no

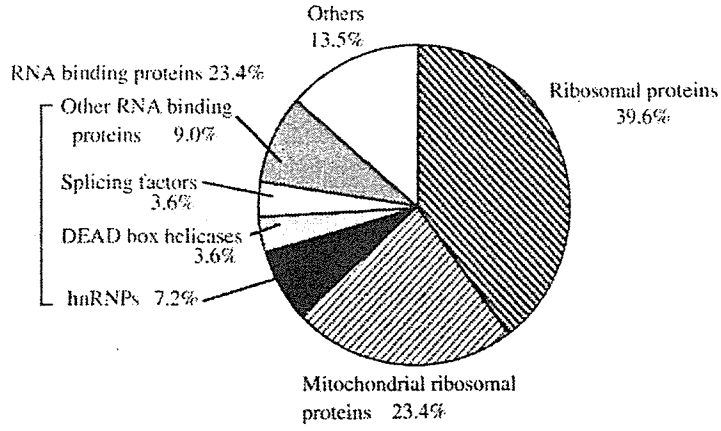

FIG. 1. **Classification of the 111 proteins identified as components of the SYNCRIP-associated protein complexes in 293EBNA cells.** Detailed compositions of each class are shown in supplemental Table SI.

changes in the microtubules or actin structure from control cells exposed to 0.1–0.3% Me_2SO (data not shown).

RESULTS

Proteomic Analysis of SYNCRIP-associated Proteins—Proteins associated with SYNCRIP were isolated by immunoprecipitation from human 293EBNA cells expressing FLAG-tagged SYNCRIP by using anti-FLAG antibody. The 111 proteins listed in supplemental Table SI were identified as components of protein complexes containing FLAG-tagged SYNCRIP. Among these 111 proteins, 44 were identified as ribosomal proteins (39.6%) and 26 were mitochondrial ribosomal proteins (23.4%), which are encoded by nuclear genes and synthesized in the cytosol (36) (Fig. 1 and supplemental Table SI). In addition, 26 RNA-binding proteins (23.4%) including 8 hnRNPs (7.2%), 4 DEAD box helicases (3.6%), and 4 splicing factors (3.6%) were also identified as SYNCRIP-associated proteins. These results suggest that SYNCRIP preferentially associates with protein complexes involved in mRNA processing and translation.

The Distribution and Dynamics of SYNCRIP in Hippocampal Neurons—mRNA granules, the ribonucleoprotein complexes present in neuronal dendrites, have been reported to contain ribosomes and other components of translation machinery (9, 12, 13) as well as a number of RNA-binding proteins (14–18). The above results of proteomic analysis in 293EBNA cells indicate that SYNCRIP preferentially associates with the major component of mRNA granules, that is, ribosomal proteins and RNA-binding proteins (Fig. 1, supplemental Table SI). In addition, SYNCRIP itself has the ability to bind to RNA, preferentially to poly(A) and poly(U) sequences *in vitro* (19, 22, 23). These findings led us to hypothesize that SYNCRIP is a component of the mRNA granules in neuronal dendrites.

To test this hypothesis, we investigated the expression pattern and dynamics of SYNCRIP in the dendrites of rat hippocampal neurons. Expression of SYNCRIP within the hippocampus of rats was investigated by immunohistochemistry using anti-SYCNRIP-N antibodies. SYNCRIP was expressed in the pyramidal cell layer and granular cell layer (Fig. 2*A*), and SYNCRIP signals were mainly observed in the cell bodies of hippocampal neurons (Fig. 2*B*). In addition, the proximal dendrites of pyramidal cells were also labeled with the SYNCRIP antibody (Fig. 2*B*, *arrowheads*). To investigate the localization and dynamics of SYNCRIP in detail, we transfected cultured rat hippocampal neurons with plasmid DNAs encoding mouse SYNCRIP (19) tagged with GFP (GFP-SYNCRIP). To confirm that GFP-SYNCRIP reflects the localization of endogenous SYNCRIP in cultured hippocampal neurons, we compared the immunocytochemical patterns of endogenous SYNCRIP and

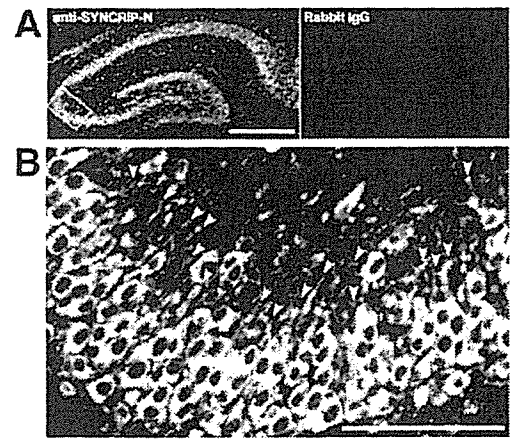

FIG. 2. **Distribution pattern of endogenous SYNCRIP in rat hippocampus.** *A*, *left*, immunohistochemistry with anti-SYNCRIP-N antibody. *Right*, control experiment using nonspecific rabbit IgG. Strong signals for endogenous SYNCRIP were found in the pyramidal and granular layers. *Scale bar*, 500 μm. *B*, a high magnification image of the *boxed* region in *A*. As well as the cell bodies, proximal dendrites of pyramidal neurons were also labeled by anti-SYNCRIP-N antibody (*arrowheads*). Images were taken with a confocal microscope. *Scale bar*, 100 μm.

the distribution of GFP-SYNCRIP signals. Endogenous SYNCRIP was distributed in the dendrites as well as in the cell body of cultured hippocampal neurons (Fig. 3*A*, *left*) as was observed in native tissue. SYNCRIP was found in granules of various sizes in the dendrites (Fig. 3*A*, *right*, *arrowheads*). GFP-SYNCRIP also exhibited a distribution pattern very similar to that of endogenous SYNCRIP (Fig. 3*B*), indicating that the expression pattern of GFP-SYNCRIP reliably reflects that of endogenous SYNCRIP in cultured neurons.

Time-lapse microscopy with a CCD camera revealed that some of the granules labeled with GFP-SYNCRIP traveled within the dendrites (Fig. 4*A* and supplemental Movie 1). Granules labeled with GFP-SYNCRIP moved along the dendrite in both anterograde (to the periphery) and retrograde (to the soma) directions, and a change in direction of movement was observed in some granules (Fig. 4*B*). Double labeling of GFP-SYNCRIP with Texas Red-dextran, which is a marker for endosomes and lysosomes, indicated that the mobile GFP-SYNCRIP-positive granules were not part of the endosome-lysosomal system because GFP-SYNCRIP did not overlap with the Texas Red-dextran signal in either the cell bodies or the dendrites (data not shown). The velocity profile of the GFP-SYN-

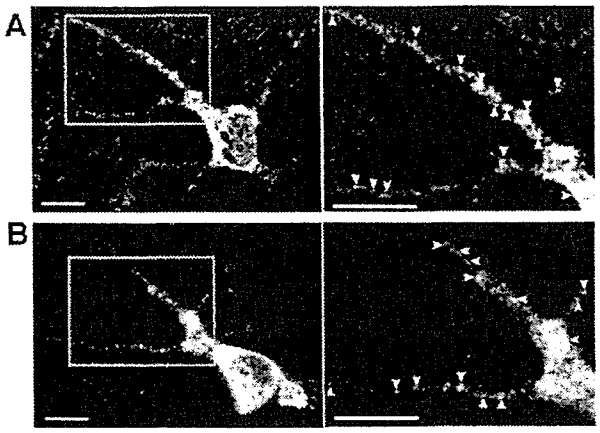

FIG. 3. **The endogenous SYNCRIP protein and expressed GFP-SYNCRIP showed comparable expression patterns in cultured rat hippocampal neurons.** *Right images* are high magnification images of the *boxed region* in the *left images*. *A*, immunolabeling of endogenous SYNCRIP using anti-SYNCRIP-N antibody. *B*, a living cell expressing GFP-SYNCRIP. In both images, many granular structures were observed in dendrites (*arrowheads*). All the images were taken with a confocal microscope. *Scale bars*, 10 μm.

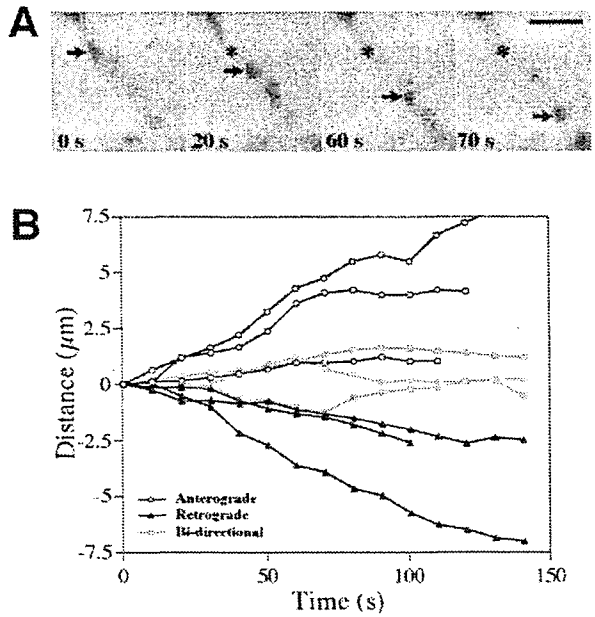

FIG. 4. **Movement of GFP-SYNCRIP-positive granules.** *A*, time-lapse imaging of GFP-SYNCRIP-positive granules in the dendrite recorded with a CCD camera. *Arrows* indicate a moving granule, and *asterisks* indicate the original position of the granule at 0 s. *Scale bar*, 2 μm. *B*, representative movement patterns of GFP-SYNCRIP-positive granules. The net movement of each vesicle (μm) was plotted against time (s). *Anterograde* (positive direction) is the movement from the cell body toward the periphery, and *Retrograde* (negative direction) is the opposite movement. The time-lapse interval was 10 s.

CRIP-positive granules is shown in Fig. 5 (*No drug treatment*). The average velocity of the vesicle movements was about 0.05 μm/s in both the anterograde and retrograde directions as shown in Table I, and the maximum velocity of GFP-SYNCRIP movement was 0.37 μm/s. Interestingly, the speed of SYNCRIP movement was similar to that reported for mRNA granule movement (~0.1 μm/s (9); ~0.1 μm/s (37); 0.03~0.05 μm/s (38)).

The movements of mRNA granules have been reported to be

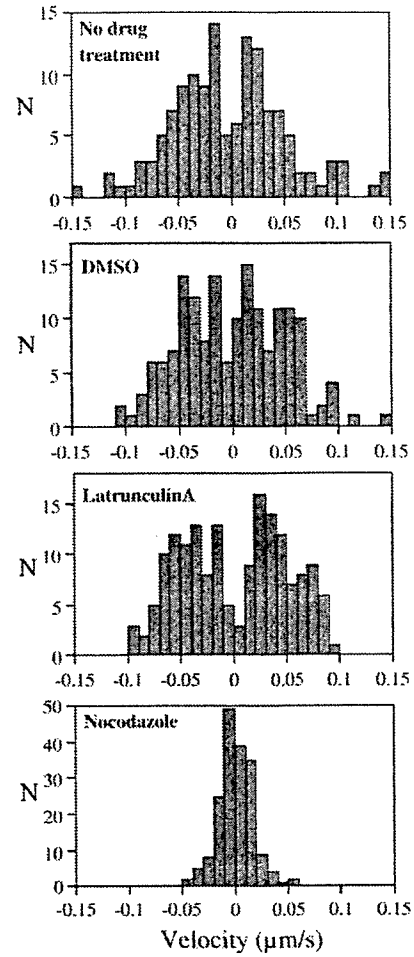

FIG. 5. **Velocity profiles of the GFP-SYNCRIP-positive granules with or without drug treatments.** *N* indicates the number of events, *i.e.* consecutive mono-directional movements. Positive velocity corresponds to the anterograde movement, and negative velocity corresponds to the retrograde movement. *DMSO*, Me_2SO.

mainly dependent on microtubules (9, 18, 35, 37–39). To determine whether microtubules are also involved in the movement of SYNCRIP-positive granules, we tested the effects of drugs that disrupt these cytoskeletal components on the velocity of granule movement. After confirming that these drugs were effective in cultured rat hippocampal neurons by immunocytochemical staining with anti-tubulin antibody (for microtubules) and Alexa 594-phalloidin (for actin filaments) (data not shown), nocodazole (30 μg/ml) and latrunculin A (1 μg/ml) were used to disrupt microtubules and actin filaments, respectively. Neither substance had a major effect on the distribution pattern or number of granules labeled with GFP-SYNCRIP. Latrunculin A did not have a significant effect on the velocity of GFP-SYNCRIP-positive granules in comparison with control cells exposed to 0.3% Me_2SO ($p > 0.1$, *t* test, and Mann-Whitney *U* test). However, nocodazole significantly decreased the velocity of GFP-SYNCRIP-positive granules by ~70% in both directions compared with control cells ($p < 0.001$, *t* test and Mann-Whitney *U* test, Fig. 5 and Table I). These results suggest that the transport of SYNCRIP-positive granules is highly dependent on microtubules and that the contribution of the actin cytoskeleton is minor, which is consistent with previous reports for the transport of mRNA granules.

TABLE I
Effects of drug treatment on the velocity of the movement of GFP-SYNCRIP-positive granules

Drug	Anterograde	Retrograde
	μm/s	*μm/s*
No drug treatment	0.050 ± 0.051 (n = 66)[a]	0.055 ± 0.058 (n = 75)
Me_2SO	0.041 ± 0.028 (n = 84)	0.041 ± 0.025 (n = 79)
Latrunculin A	0.045 ± 0.023 (n = 85)	0.043 ± 0.023 (n = 82)
Nocodazole	0.014 ± 0.010 (n = 90)[b]	0.012 ± 0.009 (n = 89)[b]

[a] Values show average ± S.D.
[b] $p < 0.001$ (t test, Mann-Whitney U test)

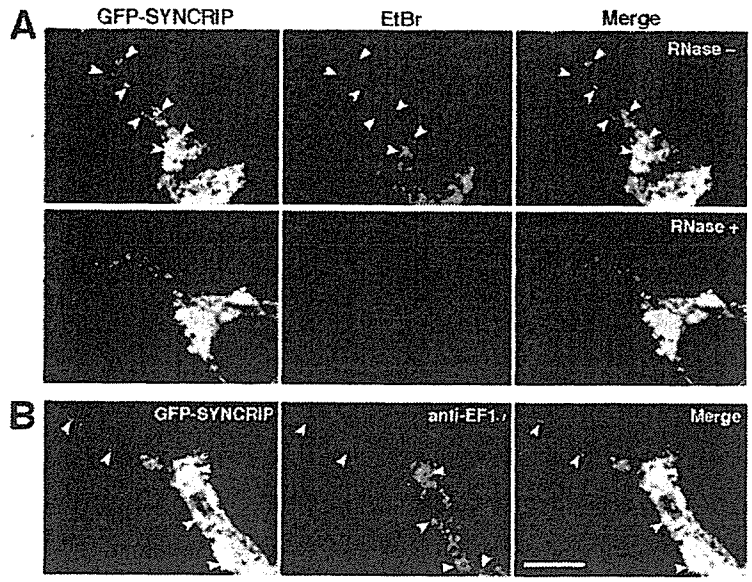

FIG. 6. **The GFP-SYNCRIP protein co-localized with the components of mRNA granules.** *A*, RNA labeling of GFP-SYNCRIP-expressing neurons with EtBr. *Top*, EtBr signals overlapped with GFP-SYNCRIP-positive granules (*arrowheads*). *Bottom*, EtBr signals were abolished by treatment with RNase A. *B*, double-labeling with GFP-SYNCRIP and endogenous EF1α, a marker for mRNA granules. Endogenous EF1α was found on the GFP-SYNCRIP-labeled granules (*arrowheads*). Images were taken with a confocal microscope. The *scale bar* indicates 10 μm.

SYNCRIP Was Co-localized with Dendritic RNAs and Markers of mRNA Granules—We then investigated whether the distribution of SYNCRIP overlaps with that of RNA and mRNA granule markers in dendrites of cultured hippocampal neurons. Dendritic RNAs were labeled with EtBr as described previously (35). The EtBr signal was completely abolished by RNase treatment, indicating that it was specific for RNA (Fig. 6*A*, *bottom*). In the absence of RNase, EtBr labeled granular structures in the cell bodies and dendrites, which overlapped with the most of the SYNCRIP-positive granules (Fig. 6*A*, *top*).

We also investigated whether GFP-SYNCRIP was co-localized with protein components of mRNA granules, *i.e.* EF1α (9) and staufen (15, 40). Immunocytochemistry using anti-EF1α antibody revealed that GFP-SYNCRIP-positive granules were co-localized with endogenous EF1α (Fig. 6*B*). However, we were not able to perform immunocytochemistry for staufen, because no specific antibody against rat staufen was available. Instead, we used GFP-tagged human staufen1 (GFP-hStau1), which is transported within dendrites as a component of mRNA granules (37). GFP-hStau1 was co-expressed with SYNCRIP tagged with monomeric RFP (mRFP-SYCNRIP), whose behavior was indistinguishable from that of GFP-SYNCRIP (data not shown). mRFP-SYNCRIP was co-localized with GFP-hStau1 in granules (Fig. 7*A*), and we confirmed that the GFP-hStau1-positive granules contained endogenous SYNCRIP by immunocytochemistry (supplemental data S1). These results strongly indicate that SYNCRIP is a component of the mRNA granule in neurons.

SYNCRIP Is a Component of Moving mRNA Granules Containing the 3′-UTR of IP_3R1 mRNA—Fig. 7*B* and supplemental Movie 2 show representative time-lapse images of a dendrite from a hippocampal neuron expressing mRFP-SYNCRIP and GFP-hStau1. The mRFP-SYNCRIP signal completely overlapped with that of GFP-hStau1 throughout the movement, indicating that SYNCRIP is a component of the "moving" mRNA granules.

Finally, we investigated whether the SYNCRIP-positive granules actually transport meaningful sets of mRNAs. The mRNA of IP_3R1 is expressed in central nervous system neurons, including hippocampal neurons (41). In addition, IP_3R1 mRNA has been shown to be present in the dendrites of cerebellar Purkinje cells and neocortical neurons (41, 42). Because a sequence homologous to the hnRNP A2 response element (A2RE, GCCAAGGAGCCAGAGAGCATG), which is included in a subset of dendritically localized mRNAs generally transported as components of mRNA granules (18, 43), is found in the 3′-UTR of IP_3R1 mRNA (GCAAATGAGGCAGAGGGACTC, bases identical to those of A2RE are underlined), it is a candidate for a component of mRNA granules. We visualized the 3′-UTR of IP_3R1 mRNA in living neurons by a GFP-based mRNA labeling technique that was first reported in yeast (29) and was used later to visualize several mRNAs in neuronal dendrites (17, 38). We prepared two plasmids, with one (NLS-MS2-Venus) containing the coding sequences of the single-stranded RNA phage capsid protein MS2 fused with Venus (a brighter variant of yellow fluorescent protein (30)) and an NLS. The other plasmid (IP_3R1 3′-UTR-MS2bs) contained 12 repeats of the MS2 binding sequence, each of which encoded a 17-nucleotide RNA stem loop fused with the 3′-UTR of IP_3R1 mRNA (bases 8579–9041). When these plasmids were co-transfected into hippocampal neurons, small bright granules were seen in the dendrites (Fig. 8*A*, *top*), whereas diffuse, not punctate staining was seen in the dendrites in a control experiment in which NLS-MS2-Venus alone was transfected (Fig. 8*A*, *bot-*

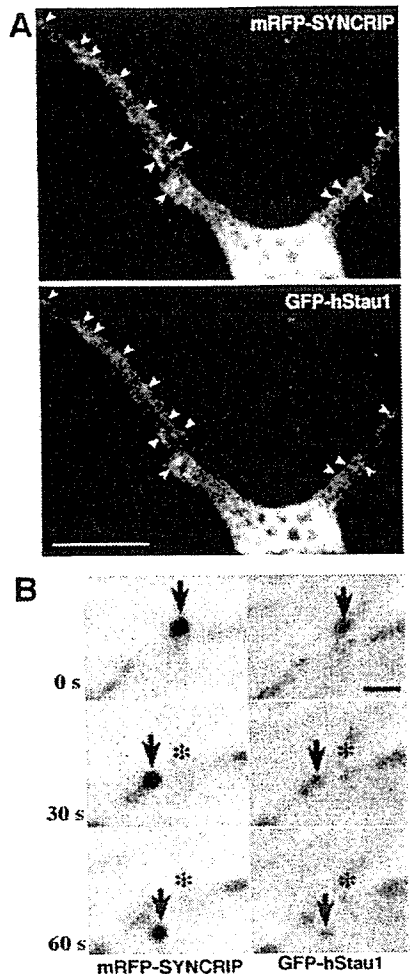

FIG. 7. **mRFP-SYNCRIP proteins were incorporated in motile mRNA granules.** *A*, double labeling of neurons with mRFP-SYNCRIP and GFP-tagged human staufen (GFP-hStau1). mRFP-SYNCRIP and GFP-hStau1 co-localized on the same granules (*arrowheads*). Images were taken with a confocal microscope. *Scale bar*, 10 μm. *B*, time-lapse images of a granule containing mRFP-SYNCRIP and GFP-hStau1 in a dendrite. *Left*, consecutive frames showing a mRFP-SYNCRIP signal. *Right*, corresponding frames showing a GFP-hStau1 signal. *Arrows* indicate a moving granule, and *asterisks* indicate the original position of the granule at 0 s. Note that both mRFP-SYNCRIP and GFP-hStau1 labeled the same moving granule. *Scale bar*, 2 μm.

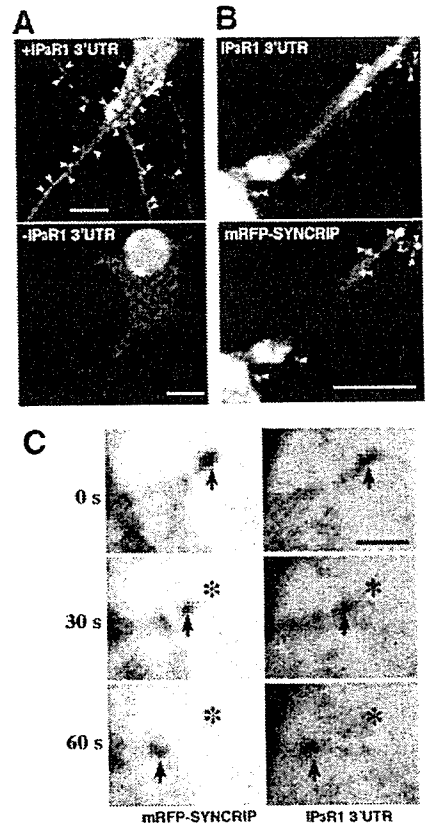

FIG. 8. **3′-UTR of IP_3R1 mRNA was co-transported with mRFP-SYNCRIP.** *A*, to visualize the 3′-UTR of IP_3R1 mRNA, cultured neurons were co-transfected with plasmid DNAs encoding 3′-UTR of mouse IP_3R1 mRNA fused with 12 copies of the MS2 binding sequence (IP_3R1 3′-UTR-MS2bs) and Venus fused with the MS2 and NLS (NLS-MS2-Venus). IP_3R1 3′-UTR mRNAs expressed in neurons was distributed as granular structures (*top*, *arrowheads*). On the other hand, a diffuse staining pattern was observed when NLS-MS2-Venus alone was transfected (*bottom*). *B*, double labeling of cultured neurons with 3′-UTR of IP_3R1 mRNA and mRFP-SYNCRIP. Many of the Venus-positive granules were mRFP-SYNCRIP-positive (*arrowheads*). Images in *A* and *B* were taken with a confocal microscope. *Scale bars*, 10 μm. *C*, movement of a granule containing mRFP-SYNCRIP and 3′-UTR of IP_3R1 mRNA in a dendrite. *Left*, consecutive frames showing a mRFP-SYNCRIP signal. *Right*, corresponding frames showing a 3′-UTR of IP_3R1 mRNA signal detected by Venus. A CCD camera was used. *Arrows* indicate a moving granule, and *asterisks* indicate the original position of the granule at 0 s. Note that both mRFP-SYNCRIP and the 3′-UTR of IP_3R1 mRNA were on the same moving granule. *Scale bar*, 2 μm.

tom). These granules were also labeled with mRFP-SYNCRIP when mRFP-SYNCRIP was further added to the co-transfected plasmids (Fig. 8*B*). A multicolor time-lapse study revealed that the movement of the IP_3R1 3′-UTR mRNA signal coincided with that of the mRFP-SYNCRIP (Fig. 8*C* and supplemental Movie 3). Taken together, these findings indicate that SYNCRIP is a component of mRNA granules that at least transports IP_3R1 mRNA.

DISCUSSION

In the proteomics study we showed that the SYNCRIP-associated complexes in 293EBNA cells contain at least 111 proteins, some of which seem to be responsible for mRNA processing and translation (Fig. 1 and supplemental Table SI). Cytoplasmic ribosomal proteins and RNA binding proteins such as hnRNP A2/B1, zip code-binding protein 1 (IGF-II mRNA-binding protein 1), and hnRNP U, which are the components of mRNA granules (17, 18, 44), were also detected as major SYNCRIP-associated proteins, and this fact raised the possibility that SYNCRIP plays roles as a component of mRNA granules in the neurons. Very recently, a screening study for RNase-sensitive granules that associate with motor protein kinesin revealed that SYNCRIP is one of the components of mRNA transporting granule (44). Moreover, proteomic and immunoelectron microscopic analyses showed that SYNCRIP is included in mRNA granules purified from rat brains.[2] Our new lines of evidence further strengthen these reports that SYNCRIP is a component of mRNA granules. SYNCRIP were distributed in dendrites of hippocampal neurons as a granular structure (Figs. 2 and 3), and the SYNCRIP-containing granules were transported bi-directionally at a speed of ~0.05 μm/s in a microtubule-dependent manner (Fig. 4 and Table I), as was

[2] W. S. Sossin and P. S. McPherson, Montreal Neurological Institute, McGill University, Quebec, Canada, personal communication.

previously reported for mRNA granule dynamics (9, 18, 35, 37–39, 44). SYNCRIP in the dendrite co-localized with RNA and the component of mRNA granules (Figs. 5–7) and was co-transported with IP_3R1 mRNA (Fig. 8). The molecular mechanism underlying the recruitment of SYNCRIP into mRNA granules remains unknown. One possibility is that SYNCRIP interacts with poly(A) or AU-rich regions that are generally present in the 3′ region of mRNAs, as was supported by the fact that SYNCRIP interacts directly with poly(A) and poly(U) *in vitro* (19, 22, 23). Another possibility is that SYNCRIP is bound to mRNA granules as a component of a protein complex as is reported for a human homolog of SYNCRIP in a non-neuronal cell (24). Clarification of the binding relations among the components of mRNA granules may be required to investigate these possibilities.

It is interesting that a number of mitochondrial ribosomal proteins associated with SYNCRIP in 293EBNA cells (Fig. 1 and supplemental Table SI). However, SYNCRIP was not found in mitochondria either in the human kidney cell line and the cultured hippocampal neuron (data not shown). SYNCRIP might associate with mitochondrial ribosomal proteins in the cytoplasm and have indirect roles in protein synthesis in mitochondria, but further study is required to test this possibility.

Microtubule-based motor proteins kinesin and dynein are possibly responsible for the transport of SYCNRIP-positive mRNA granule, since they were co-purified with SYNCRIP-containing mRNA granules (44).[2] mRNA granules that contain cytoplasmic polyadenylation element-binding protein has also been shown to be co-localized with molecular motor kinesin and dynein (39). Bi-directional movement of GFP-SYNCRIP-positive granules (Fig. 4) could be explained by mixed polarity of the dendritic microtubules (45) or by coordination of multiple, opposite-directed motor proteins. In the present study, actin filaments were shown to contribute little to the transport of SYNCRIP (Fig. 5 and Table I), which has also been reported to be the case for the movement of hnRNP A2-positive mRNA granules (18). Although actin filaments seem less involved in the transport of mRNA granules, an actin motor myosin V is shown to be a component of the mRNA/protein complex containing staufen and fragile X mental retardation protein (46). Our results do not necessarily exclude a possible association of SYNCRIP-containing mRNA granules with actin filaments.

The speed of GFP-SYNCRIP-positive granule movement (~0.05 μm/s, Fig. 5) was comparable with that of mRNA granules visualized by SYTO14 (0.1 μm/s, 9), of staufen-containing granules (~0.1 μm/s, 37), and of mRNA granules containing the 3′-UTR of CaMKIIα mRNA (0.03~0.05 μm/s (38)). However, the speed of GFP-SYNCRIP was much slower than that of zip code-binding protein 1 and β-actin mRNA-positive granules, which move at an average velocity of ~1.0 μm/s (17), which exceeds the maximum speed of GFP-SYNCRIP movement (0.37 μm/s). This result suggests a possibility that SYNCRIP is not involved in mRNA granules that are transported at a fast speed. Variety in the transport speeds of mRNA granules may reflect the heterogeneity in mRNA granules that has been proposed recently (47).[2] In addition to the differences in the motor proteins interacting with each subset of mRNA granules, interaction between mRNA granules and organelles may modulate the dynamics of mRNA granules. mRNA granules containing staufen and fragile X mental retardation protein are reported to associate with rough endoplasmic reticulum (46), and this association may affect the transport of mRNA granules. Further work is required to understand the heterogeneity in mRNA granules and their transport.

In this study, we have demonstrated that 3′-UTR of IP_3R1 is co-transported with SYNCRIP as mRNA granules (Fig. 8). Although IP_3R1 mRNA was previously shown to be present in the dendrites of cerebellar Purkinje cells and neocortical neurons (41, 42), the mechanism underlying the dendritic distribution of IP_3R1 mRNA has never been elucidated. This study suggests that IP_3R1 mRNA may be delivered into the dendrites via mRNA granule transport and that 3′-UTR of IP_3R1 mRNA may contain a targeting signal to dendritic mRNA granules, as is known for other dendritic localized mRNAs. IP_3R plays an important role, such as induction of synaptic plasticity in neuronal dendrites (48–50). The dendritic localization and local translation of CaMKIIα mRNA are responsible for the delivery of the kinase and for the induction of synaptic plasticity (51). The dendritic transported mRNA granules containing IP_3R1 mRNA may also be important for accurate delivery of IP_3R1 proteins into the post-synapse and for the induction of synaptic plasticity.

Although the physiological roles of SYNCRIP are still poorly understood even in non-neuronal cells, some interesting properties of SYNCRIP have been reported. Because SYNCRIP is a component of a protein complex that stabilizes c-*fos* mRNA (24), it is possible that SYNCRIP also stabilizes mRNAs during their transport in dendrites. Insulin stimulation and osmotic shocks are reported to induce phosphorylation of tyrosine residues of SYNCRIP, and the RNA binding activity of SYNCRIP is modified by phosphorylation (22, 23). Insulin is present in the brain (for review, see Ref. 52), and insulin receptor tyrosine kinases are abundant in the hippocampus, especially in neuronal dendrites, including synapses (53, 54). In addition, overexpressed fibroblast growth factor receptor 1, a receptor tyrosine kinase that is expressed in hippocampal neurons (55), is also shown to phosphorylate a human homolog of SYNCRIP (NSAP1) on its tyrosine 373, which is located in the third RNA recognition motif domain (56). These studies raise intriguing possibilities that the turnover or translation of mRNAs contained within mRNA granules could be controlled by the insulin- or fibroblast growth factor-dependent phosphorylation of SYNCRIP in hippocampal neurons. Elucidating the functions of SYNCRIP and its regulatory mechanism in mRNA granules may provide an important key for understanding the temporal and spatial regulation of the local translation of mRNA involved in the induction of synaptic plasticity.

Acknowledgments—We thank Dr. R. Tsien (University of California, San Diego, CA) for the gift of monomeric RFP, Dr. S. Sugano (The Institute of Medical Science, The University of Tokyo, Tokyo, Japan) for the gift of a cDNA clone for human staufen1 (HEP22160), Dr. R. Singer (Saint Mary's University, Nova Scotia, Canada) for the gift of pGA14-MS2-GFP, Dr. A. Miyawaki (RIKEN, Saitama, Japan) for the gift of CS2-Venus, and Drs. McPherson and Sossin (Montreal Neurological Institute, McGill University, Quebec, Canada) for valuable discussions. We also thank M. Iwai (The University of Tokyo) for assistance with plasmid construction.

REFERENCES

1. Bashirullah, A., Cooperstock, R. L., and Lipshitz, H. D. (1998) *Annu. Rev. Biochem.* **67,** 335–394
2. Kuhl, D., and Skehel, P. (1998) *Curr. Opin. Neurobiol.* **8,** 600–606
3. Tiedge, H., Bloom, F. E., and Richter, D. (1999) *Science* **283,** 186–187
4. Kiebler, M. A., and DesGroseillers, L. (2000) *Neuron* **25,** 19–28
5. Kacharmina, J. E., Job, C., Crino, P., and Eberwine, J. (2000) *Proc. Natl. Acad. Sci. U. S. A.* **97,** 11545–11550
6. Aakalu, G., Smith, W. B., Nguyen, N., Jiang, C., and Schuman, E. M. (2001) *Neuron* **30,** 489–502
7. Job, C., and Eberwine, J. (2001) *Proc. Natl. Acad. Sci. U. S. A.* **98,** 13037–13042
8. Steward, O., and Schuman, E. M. (2003) *Neuron* **40,** 347–359
9. Knowles, R. B., Sabry, J. H., Martone, M. E., Deerinck, T. J., Ellisman, M. H., Bassell, G. J., and Kosik, K. S. (1996) *J. Neurosci.* **16,** 7812–7820
10. Racca, C., Gardiol, A., and Triller, A. (1997) *J. Neurosci.* **17,** 1691–1700
11. Wanner, I., Baader, S. L., Brich, M., Oberdick, J., and Schilling, K. (1997) *Histochem. Cell Biol.* **108,** 345–357
12. Tiedge, H., and Brosius, J. (1996) *J. Neurosci.* **16,** 7171–7181
13. Torre, E. R., and Steward, O. (1996) *J. Neurosci.* **16,** 5967–5978
14. Feng, Y., Gutekunst, C. A., Eberhart, D. E., Yi, H., Warren, S. T., and Hersch, S. M. (1997) *J. Neurosci.* **17,** 1539–1547
15. Kiebler, M. A., Hemraj, I., Verkade, P., Köhrmann, M., Fortes, P., Marion, R. M., Ortin, J., and Dotti, C. G. (1999) *J. Neurosci.* **19,** 288–297

16. Severt, W. L., Biber, T. U., Wu, X., Hecht, N. B., DeLorenzo, R. J., and Jakoi, E. R. (1999) *J. Cell Sci.* **112,** 3691–3702
17. Tiruchinapalli, D. M., Oleynikov, Y., Kelic, S., Shenoy, S. M., Hartley, A., Stanton, P. K., Singer, R. H., and Bassell, G. J. (2003) *J. Neurosci.* **23,** 3251–3261
18. Shan, J., Munro, T. P., Barbarese, E., Carson, J. H., and Smith, R. (2003) *J. Neurosci.* **23,** 8859–8866
19. Mizutani, A., Fukuda, M., Ibata, K., Shiraishi, Y., and Mikoshiba, K. (2000) *J. Biol. Chem.* **275,** 9823–9831
20. Harris, C. E., Boden, R. A., and Astell, C. R. (1999) *J. Virol.* **73,** 72–80
21. Mourelatos, Z., Abel, L., Yong, J., Kataoka, N., and Dreyfuss, G. (2001) *EMBO J.* **20,** 5443–5452
22. Hresko, R. C., and Mueckler, M. (2000) *J. Biol. Chem.* **275,** 18114–18120
23. Hresko, R. C., and Mueckler, M. (2002) *J. Biol. Chem.* **277,** 25233–25236
24. Grosset, C., Chen, C. Y., Xu, N., Sonenberg, N., Jacquemin-Sablon, H., and Shyu, A. B. (2000) *Cell* **103,** 29–40
25. Yanagida, M., Shimamoto, A., Nishikawa, K., Furuichi, Y., Isobe, T., and Takahashi, N. (2001) *Proteomics* **1,** 1390–1404
26. Natsume, T., Yamauchi, Y., Nakayama, H., Shinkawa, T., Yanagida, M., Takahashi, N., and Isobe, T. (2002) *Anal. Chem.* **74,** 4725–4733
27. Yanagida, M., Hayano, T., Yamauchi, Y., Shinkawa, T., Natsume, T., Isobe, T., and Takahashi, N. (2004) *J. Biol. Chem.* **279,** 1607–1614
28. Campbell, R. E., Tour, O., Palmer, A. E., Steinbach, P. A., Baird, G. S., Zacharias, D. A., and Tsien, R. Y. (2002) *Proc. Natl. Acad. Sci. U. S. A.* **99,** 7877–7882
29. Bertrand, E., Chartrand, P., Schaefer, M., Shenoy, S. M., Singer, R. H., and Long, R. M. (1998) *Mol. Cell* **2,** 437–445
30. Nagai, T., Ibata, K., Park, E. S., Kubota, M., Mikoshiba, K., and Miyawaki, A. (2002) *Nat. Biotechnol.* **20,** 87–90
31. Higgins, D., and Banker, G. (1998) in *Culturing Nerve Cells* (Banker, G., and Goslin, K., eds) pp. 37–78, MIT Press, Cambridge, MA
32. Bannai, H., Inoue, T., Nakayama, T., Hattori, M., and Mikoshiba, K. (2004) *J. Cell Sci.* **117,** 163–175
33. Köhrmann, M., Haubensak, W., Hemraj, I., Kaether, C., Leβmann, V. J., and Kiebler, M. A. (1999) *J. Neurosci. Res.* **58,** 831–835
34. Blanpied, T. A., Scott, D. B., and Ehlers, M. D. (2002) *Neuron* **36,** 435–449
35. Tang, S. J., Meulemans, D., Vazquez, L., Colaco, N., and Schuman, E. (2001) *Neuron* **32,** 463–475
36. O'Brien, T. W. (2002) *Gene (Amst.)* **286,** 73–79
37. Köhrmann, M., Luo, M., Kaether, C., DesGroseillers, L., Dotti, C. G., and Kiebler, M. A. (1999) *Mol. Biol. Cell* **10,** 2945–2953
38. Rook, M. S., Lu, M., and Kosik, K. S. (2000) *J. Neurosci.* **20,** 6385–6393
39. Huang, Y. S., Carson, J. H., Barbarese, E., and Richter, J. D. (2003) *Genes Dev.* **17,** 638–653
40. Mallardo, M., Deitinghoff, A., Muller, J., Goetze, B., Macchi, P., Peters, C., and Kiebler, M. A. (2003) *Proc. Natl. Acad. Sci. U. S. A.* **100,** 2100–2105
41. Furuichi, T., Simon-Chazottes, D., Fujino, I., Yamada, N., Hasegawa, M., Miyawaki, A., Yoshikawa, S., Guenet, J. L., and Mikoshiba, K. (1993) *Receptors Channels* **1,** 11–24
42. Bagni, C., Mannucci, L., Dotti, C. G., and Amaldi, F. (2000) *J. Neurosci.* **20,** 1–6
43. Ainger, K., Avossa, D., Diana, A. S., Barry, C., Barbarese, E., and Carson, J. H. (1997) *J. Cell Biol.* **138,** 1077–1087
44. Kanai, Y., Dohmae, N., and Hirokawa, N. (2004) *Neuron* **43,** 513–525
45. Baas, P. W., Deitch, J. S., Black, M. M., and Banker, G. A. (1988) *Proc. Natl. Acad. Sci. U. S. A.* **85,** 8335–8339
46. Ohashi, S., Koike, K., Omori, A., Ichinose, S., Ohara, S., Kobayashi, S., Sato, T. A., and Anzai, K. (2002) *J. Biol. Chem.* **277,** 37804–37810
47. Duchaine, T. F., Hemraj, I., Furic, L., Deitinghoff, A., Kiebler, M. A., and DesGroseillers, L. (2002) *J. Cell Sci.* **115,** 3285–3295
48. Inoue, T., Kato, K., Kohda, K., and Mikoshiba, K. (1998) *J. Neurosci.* **18,** 5366–5373
49. Fujii, S., Matsumoto, M., Igarashi, K., Kato, H., and Mikoshiba, K. (2000) *Learn. Mem.* **7,** 312–320
50. Nishiyama, M., Hong, K., Mikoshiba, K., Poo, M. M., and Kato, K. (2000) *Nature* **408,** 584–588
51. Miller, S., Yasuda, M., Coats, J. K., Jones, Y., Martone, M. E., and Mayford, M. (2002) *Neuron* **36,** 507–519
52. Wozniak, M., Rydzewski, B., Baker, S. P., and Raizada, M. K. (1993) *Neurochem. Int.* **22,** 1–10
53. Hill, J. M., Lesniak, M. A., Pert, C. B., and Roth, J. (1986) *Neuroscience* **17,** 1127–1138
54. Abbott, M. A., Wells, D. G., and Fallon, J. R. (1999) *J. Neurosci.* **19,** 7300–7308
55. Lin, S. D., and Fann, M. J. (1998) *J. Biomed. Sci.* **5,** 111–119
56. Hinsby, A. M., Olsen, J. V., Bennett, K. L., and Mann, M. (2003) *Mol. Cell. Proteomics* **2,** 29–36

Cell, Vol. 120, 85–98, January 14, 2005, Copyright ©2005 by Elsevier Inc. DOI 10.1016/j.cell.2004.11.048

Subtype-Specific and ER Lumenal Environment-Dependent Regulation of Inositol 1,4,5-Trisphosphate Receptor Type 1 by ERp44

Takayasu Higo,[1,2] Mitsuharu Hattori,[1,3,6] Takeshi Nakamura,[4] Tohru Natsume,[5] Takayuki Michikawa,[1] and Katsuhiko Mikoshiba[1,2,4,*]
[1]Department of Molecular Neurobiology
Institute of Medical Science
University of Tokyo
4-6-1 Shirokanedai, Minato-ku
Tokyo 108-8639
Japan
[2]Laboratory for Developmental Neurobiology
Brain Science Institute
RIKEN, Wako, Saitama 351-0198
Japan
[3]PRESTO
[4]Calcium Oscillation Project
ICORP, JST
Kawaguchi, Saitama 332-0012
Japan
[5]Protein Network Team
Functional Genome Group
Japan Biological Information Research Center
Koto-ku
Tokyo 135-8073
Japan

Summary

Inositol 1,4,5-trisphosphate receptors (IP_3Rs) are intracellular channel proteins that mediate Ca^{2+} release from the endoplasmic reticulum (ER) and are involved in many biological processes and diseases. IP_3Rs are differentially regulated by a variety of cytosolic proteins, but their regulation by ER lumenal protein(s) remains largely unexplored. In this study, we found that ERp44, an ER lumenal protein of the thioredoxin family, directly interacts with the third lumenal loop of IP_3R type 1 (IP_3R1) and that the interaction is dependent on pH, Ca^{2+} concentration, and redox state: the presence of free cysteine residues in the loop is required. Ca^{2+}-imaging experiments and single-channel recording of IP_3R1 activity with a planar lipid bilayer system demonstrated that IP_3R1 is directly inhibited by ERp44. Thus, ERp44 senses the environment in the ER lumen and modulates IP_3R1 activity accordingly, which should in turn contribute to regulating both intralumenal conditions and the complex patterns of cytosolic Ca^{2+} concentrations.

Introduction

The cytosolic Ca^{2+} concentration ($[Ca^{2+}]_c$) is the focal point of many signal transduction pathways and regulates a variety of cellular activities ranging from fertilization to cell death (Berridge et al., 2003). $[Ca^{2+}]_c$ is tightly regulated in terms of time, space, and amplitude, and cells extract specific information based on these parameters. Ca^{2+} ions can be supplied to the cytosol from the extracellular space or from intracellular Ca^{2+} stores, such as the endoplasmic reticulum (ER). Dysfunction of molecules involved in $[Ca^{2+}]_c$ regulation is assumed to play a major role in apoptosis (Orrenius et al., 2003) and neuropathological conditions, including Huntington's and Alzheimer's diseases (Paschen, 2003; Mattson, 2004). Inositol 1,4,5-trisphosphate receptors (IP_3Rs) are Ca^{2+} release channels on the ER that play a critical role in the generation of complex $[Ca^{2+}]_c$ patterning, e.g., Ca^{2+} waves and oscillations (Patterson et al., 2004). There are three IP_3R subtypes in birds and mammals, IP_3R1, IP_3R2, and IP_3R3, and they share basic properties but differ in terms of regulation and distribution (Taylor et al., 1999; Patterson et al., 2004). IP_3R1 is the dominant subtype in the brain (Taylor et al., 1999) and has been implicated in neuronal development (Takei et al., 1998; Xiang et al., 2002), in higher functions of the central nervous system (Inoue et al., 1998; Nishiyama et al., 2000), and in human neuropathology (Tang et al., 2003). A striking feature of IP_3Rs is the presence of very large cytosolic regions, including the IP_3 binding core (Patterson et al., 2004). The channel domain contains six transmembrane domains, and as a result there are three "loops" that reside in the ER lumen (Figure 1A). The third lumenal loop (L3) is the largest and can be divided into two subdomains. The first half, the L3V domain, has highly divergent primary sequences according to the subtype (Figure 1B), while the second half, the L3C domain, which includes the pore-forming region (Patterson et al., 2004), is almost completely conserved among types and species. Interestingly, the primary sequence of the L3V domain of each IP_3R subtype is well conserved among animal species, suggesting that this domain is involved in subtype-specific regulation. However, the function of the L3V domain remains largely unexplored.

It is evident that the intralumenal environment of the ER regulates the function of numerous proteins (Berridge et al., 2003), but how it regulates IP_3R activity remains unclear despite a great deal of research. For example, whether IP_3R is directly regulated by the Ca^{2+} concentration in the ER lumen ($[Ca^{2+}]_{ER}$) is still a matter of debate (Caroppo et al., 2003 and references therein). Calreticulin (CRT), an ER lumenal lectin with high Ca^{2+} binding capacity, regulates IP_3-induced Ca^{2+} release (IICR) (Camacho and Lechleiter, 1995; Roderick et al., 1998), but whether or not this is a direct effect on IP_3R remains unknown because CRT critically regulates the activity of sarcoendoplasmic reticulum Ca^{2+} ATPase (SERCA) 2b (Li and Camacho, 2004). Chromogranins that mainly reside in secretory granules associate with the L3C domain of IP_3Rs and modulate the activities of IP_3Rs (Thrower et al., 2003; Choe et al., 2004). However, the mechanisms by which interactions between chromogranins and IP_3Rs are regulated, and their physiological significance, remain unknown.

*Correspondence: mikosiba@ims.u-tokyo.ac.jp
[6]Present address: Department of Biomedical Science, Graduate School of Pharmaceutical Sciences, Nagoya City University, Mizuho-ku, Nagoya, Aichi 467-8603, Japan.

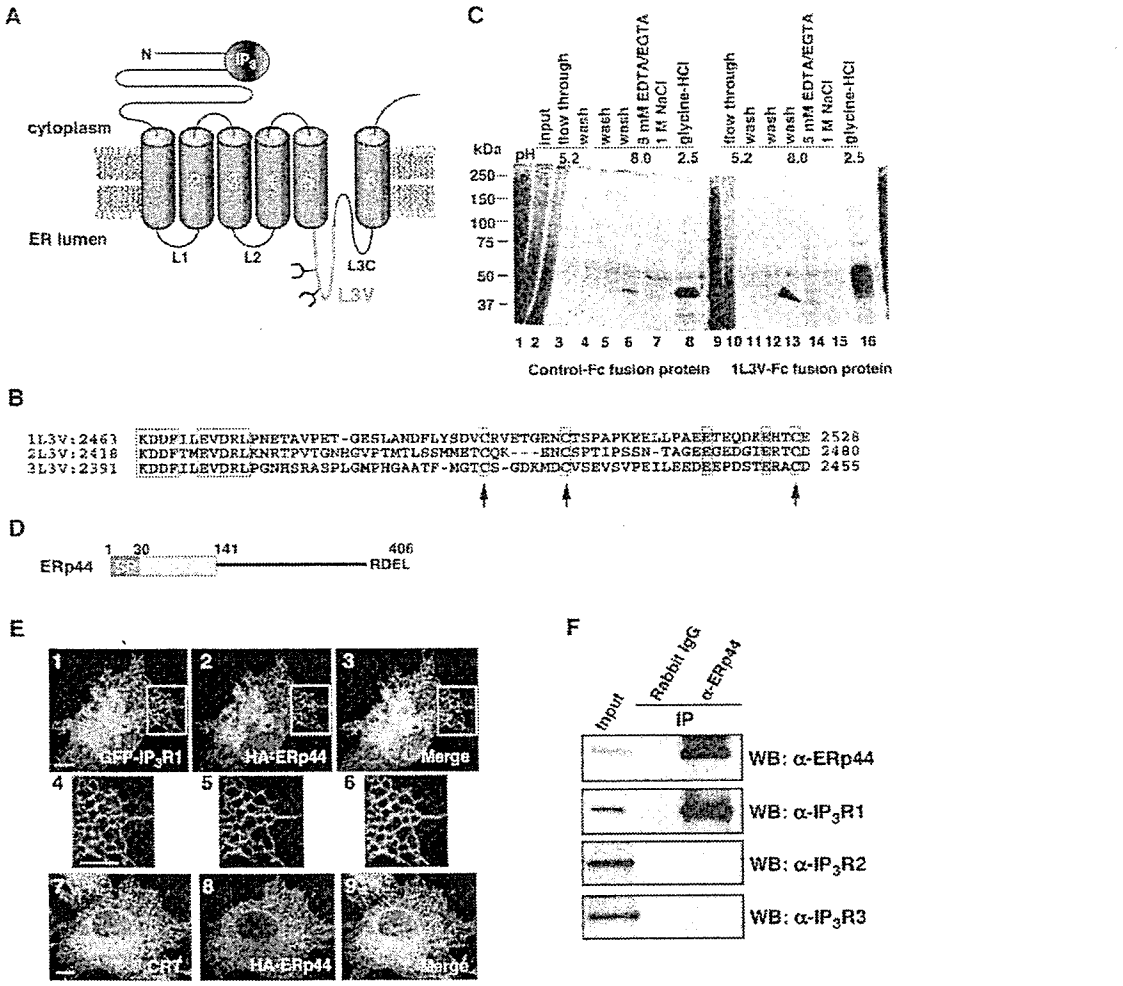

Figure 1. Identification of ERp44 as a Protein Binding to the L3V Domain of IP_3R1

(A) Schematic representation of the structure of IP_3Rs. IP_3Rs contain six membrane-spanning regions (green) and three lumenal domains, L1, L2, and L3. L3 is divided into L3V (red) and L3C. IP_3 binds to the N-terminal cytosolic region. L3V contains two glycosylation sites.

(B) Sequence comparison of the L3V of three subtypes of mouse IP_3R. Conserved amino acid residues are shown (red box). Conserved cysteine residues are indicated by arrows.

(C) Purification of 1L3V-interacting proteins. Mouse cerebellar microsomal fractions solubilized in acidic solution (pH 5.2) were added to either a control-Fc or a 1L3V-Fc column. The columns were washed with the same buffer (lanes 3 and 11), neutral buffer (lanes 4 and 5 and 12 and 13), and finally eluted with neutral buffer containing EGTA/EDTA (lanes 6 and 14), with buffer containing 1M NaCl (lanes 7 and 15), and with glycine-HCl solution (lanes 8 and 16). The arrowhead indicates the 45 kDa band that specifically binds to 1L3V-Fc, and it turned out to be ERp44.

(D) Structure of ERp44. The signal peptide (SP, aa 1–30), thioredoxin homology domain (THD, aa 31–141), and ER retention signal RDEL motif are shown.

(E) ERp44 colocalizes with IP_3R1 in the ER. COS-7 cells expressing HA-ERp44 and GFP-IP_3R1 were stained with α-HA (panels 1–3). The boxed regions in panels 1–3 are shown at increased magnification in panels 4–6, respectively. The cells expressing HA-ERp44 were stained with α-CRT and α-HA (panels 7–9). Scale bar, 10 μm.

(F) In vivo interaction between ERp44 and IP_3R1. HeLa cells were treated with a membrane-permeable crosslinker, DSP, and then solubilized. The cell lysates were subjected to IP with control rabbit IgG or α-ERp44. The lysate (Input) and IP samples were analyzed by Western blotting (WB) with indicated antibodies.

To elucidate the molecular mechanism underlying subtype-specific regulation of IP_3Rs on the ER lumen side, we searched for proteins that bind to the L3V domain of IP_3Rs. We succeeded in identifying ERp44, a thioredoxin (TRX) family protein previously implicated in oxidative protein folding, as a protein that specifically binds to the L3V domain of IP_3R1. Herein, we present strong evidence that ERp44 directly inhibits the channel activity of the IP_3R1 in a pH-, redox state-, and $[Ca^{2+}]_{ER}$-dependent manner. This is the first demonstration of negative regulation of IP_3Rs by a specific binding protein in the ER lumen. We anticipate that our results will contribute to understanding of the mechanism by which cells integrate various signals from the extracellular mi-

lieu and from the ER lumen in generating complex Ca^{2+} signaling patterns.

Results

Identification of ERp44 as a Binding Protein of the L3V Domain of IP_3R1

Our first goal was to identify proteins that bind to the L3V domain of IP_3Rs. Yeast two-hybrid screening was considered inappropriate as a method because the chemical conditions in the nucleus are completely different from those in the ER lumen. We therefore produced 1L3V-Fc protein by fusing the secretion signal and human immunoglobulin Fc domain to the N and C termini, respectively, of the L3V domain of IP_3R1 (1L3V) and then used it to prepare affinity resin. When an initial attempt under neutral conditions (pH 7.5, data not shown) failed to detect any specific 1L3V-Fc binding protein in the mouse cerebellar microsomal fraction, we performed a similar experiment under acidic conditions (pH 5.2) and succeeded in identifying two proteins that bound specifically to 1L3V-Fc (Figure 1C). Analysis of the bands by matrix-assisted laser desorption/ionization-time of flight mass spectrometry revealed the 44 kDa protein to be ERp44 (Anelli et al., 2002). The 85 kDa protein was identified as aconitase, a mitochondrial protein, and was not further characterized in this study. We then searched for binding proteins for the L3 domains of IP_3R2 and IP_3R3 (2L3V or 3L3V, respectively) in mouse brain, employing the same procedures, but detected none (data not shown).

ERp44 is an ER lumenal protein of the TRX family and contains a signal peptide, TRX-homology domain (THD), and an ER retention signal, RDEL (Figure 1D). ERp44 is widely expressed in mouse tissues (Supplemental Figure S1 at http://www.cell.com/cgi/content/full/120/1/85/DC1/). Hemagglutinin A epitope (HA)-tagged ERp44 (Anelli et al., 2002), alone or with GFP-IP_3R1, was expressed in COS-7 cells (Figure 1E). HA-ERp44 was observed as a diffuse network with GFP-IP_3R1 and endogenous CRT (Figure 1E), indicating that ERp44 colocalizes with IP_3R1 in the ER.

To confirm the interaction between IP_3R1 and ERp44, we raised polyclonal antibody against ERp44 and conducted immunoprecipitation (IP) experiments. Both IP_3R1 and ERp44 were, however, severely degraded when whole-cell lysates were prepared with acidic buffer (in which an association had been observed in the experiments shown in Figure 1C), presumably by lysosomal proteases (data not shown). To circumvent this, HeLa cells were first treated with a membrane-permeable crosslinker, dithiobis[succinimidylpropionate] (DSP), and IP was performed in neutral buffer. Under these conditions, anti-ERp44 antibody coprecipitated IP_3R1, but not IP_3R2 or IP_3R3 (Figure 1F), indicating that endogenous ERp44 and IP_3R1 exist in the same complex in vivo.

ERp44 Specifically Interacts with IP_3R1, but Not with IP_3R2 or IP_3R3, in a Condition-Dependent Manner

To further characterize the association between ERp44 and IP_3Rs, we performed a series of pulldown experiments with recombinant proteins. Glutathione (GSH) *S*-transferase (GST) and maltose binding protein (MBP) were fused to 1L3V and ERp44, respectively (Figure 2A). Under acidic conditions (pH 5.2), MBP-ERp44 specifically interacted with GST-1L3V (Figure 2B), but no interaction was observed under neutral (pH 7.2) conditions (data not shown). The pH in the ER lumen has been estimated to be almost neutral (Kim et al., 1998; Foyouzi-Youssefi et al., 2000). We reasoned that certain factor(s) may have been missed in our pulldown assays and attempted to identify conditions under which 1L3V and ERp44 interact at neutral pH.

The presence of THD in ERp44 suggests that its function is redox dependent. Both GST-1L3V and ERp44 were predominantly in their oxidized forms, and addition of the reducing reagent dithiothreitol (DTT) reduced both according to their migration patterns on SDS-PAGE under nonreducing conditions (Figure 2C). No interaction between these oxidized forms was observed at pH 7.5 (Figure 2C, lane 1), while the reduced forms did interact (Figure 2C, lane 2). It was thus concluded that ERp44 and 1L3V bind to each other in a redox-dependent manner at neutral pH.

To determine which of the protein redox states is important, the cysteine residues of the proteins were mutated. Mutation of Cys2496, Cys2504, or Cys2527 of 1L3V resulted in decreased interaction with ERp44 (Figure 2D), whereas no cysteine mutations in ERp44 affected the interaction (Supplemental Figure S2 on the *Cell* website). Taken together, these findings strongly suggest that the presence of free thiol groups in 1L3V is required for the interaction between 1L3V and ERp44 at neutral pH.

We next examined whether the interaction between ERp44 and 1L3V is dependent on the Ca^{2+} concentration. As shown in Figure 2E, the interaction diminished when the Ca^{2+} concentration was higher than 100 μM. The $[Ca^{2+}]_{ER}$ under resting conditions has been estimated to be 200–1000 μM (Meldolesi and Pozzan, 1998), suggesting that the interaction between ERp44 and IP_3R1 is enhanced when $[Ca^{2+}]_{ER}$ is decreased.

The above findings suggested that reducing and/or low $[Ca^{2+}]_{ER}$ conditions favor the interaction between ERp44 and IP_3R1. To corroborate these observations in vivo, COS-7 cells expressing HA-ERp44 and GFP-IP_3R1 were cultured in the presence or absence of DTT, and IP was performed with whole-cell lysates. Although the amount of HA-ERp44 that precipitated with anti-HA antibody was consistently less under reducing conditions for unknown reasons (Figure 2F, bottom panel), coprecipitated GFP-IP_3R1 was significantly increased (Figure 2F, middle panel). In a similar manner, cells expressing HA-ERp44 and GFP-IP_3R1 were stimulated with 10 μM (suprathreshold concentration) ATP, an activator of purinergic receptors, and the stimulation increased the amount of GFP-IP_3R1 that coprecipitated with HA-ERp44 (Figure 2G). Furthermore, Ca^{2+} depletion from the ER, elicited by thapsigargin (Tg, a SERCA inhibitor), also augmented the interaction (Figure 2H). These results indicated that dynamic changes in the ER lumenal environment affect the interaction between IP_3R1 and ERp44.

Next, to gain greater insight into the nature of the interaction, we identified the minimum 1L3V-interacting

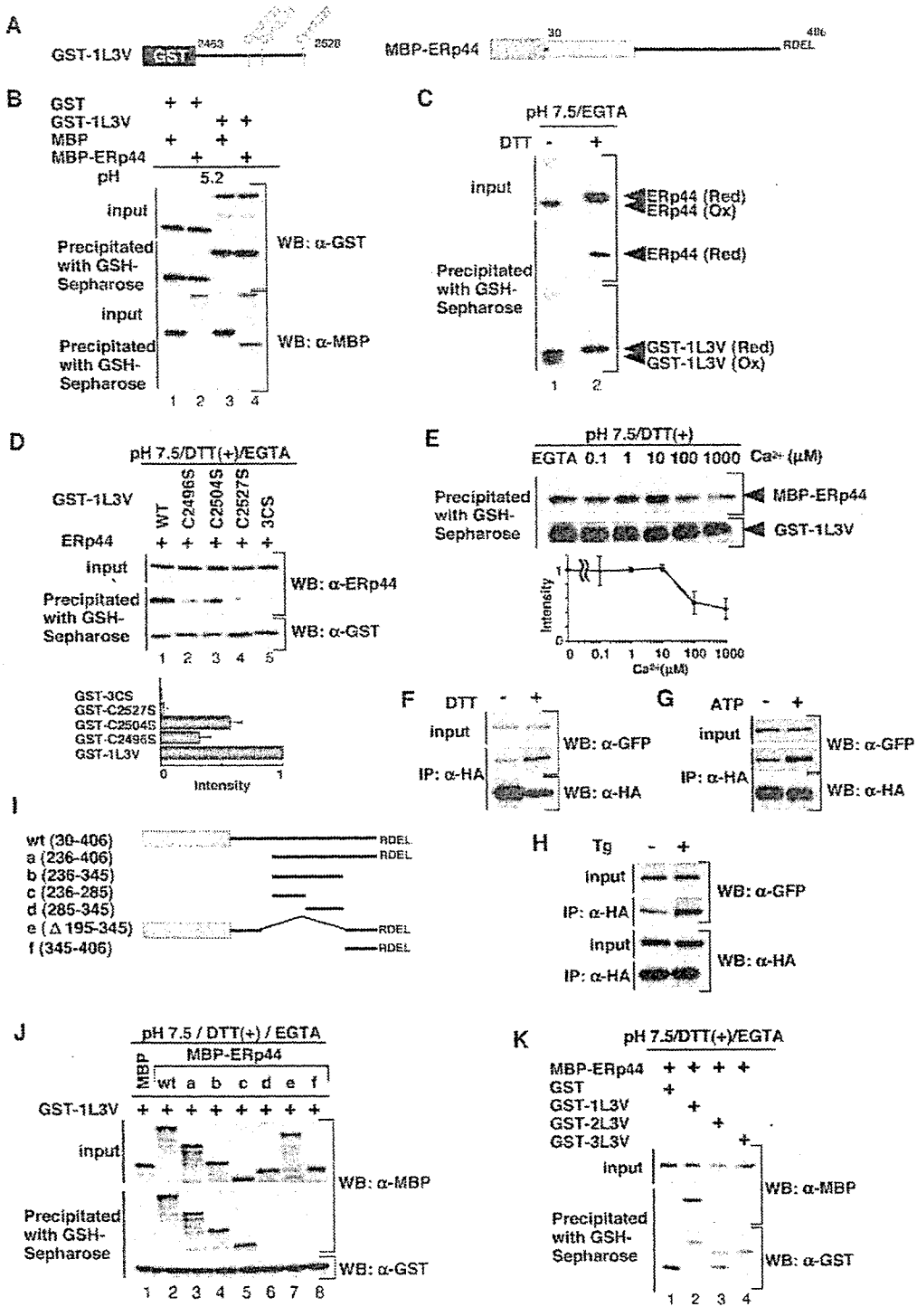

Figure 2. ERp44 Specifically Interacts with IP_3R1 in a Condition-Dependent Manner

(A) Schematic representation of recombinant proteins.

(B) ERp44 directly interacts with 1L3V in acidic buffer. Purified GST (lanes 1 and 2) or GST-1L3V (lanes 3 and 4) was incubated with purified MBP (lanes 1 and 3) or MBP-ERp44 (lanes 2 and 4) in acidic solution (pH 5.2) containing 4 mM Ca^{2+} and then precipitated with GSH-Sepharose. Precipitated proteins were subjected to Western blotting with α-GST or α-MBP.

(C) ERp44 directly interacts with 1L3V in the presence of DTT and EGTA in neutral buffer. To obtain untagged ERp44, purified GST-ERp44

region of ERp44 by fusing the full-length (without the signal sequence) or subfragments of ERp44 to MBP and testing their interactions with GST-1L3V in the presence of DTT at neutral pH. Wild-type MBP-ERp44 and MBP-ERp44 (the C-terminal half) strongly interacted with GST-1L3V (Figure 2J, lanes 2 and 3, respectively), indicating that THD is not required for the interaction. MBP-ERp44c, which contains a highly conserved glutamate-rich region but is devoid of the histidine-rich region, also bound to GST-1L3V, albeit somewhat weakly (Figure 2J, lane 5), whereas other mutants tested did not (Figure 2J, lanes 6–8). These results indicate amino acid residues 236–285 of ERp44 to be necessary and sufficient for binding to 1L3V. The primary sequence of this region has no similarities to any sequences in the database but is well conserved among species (Supplemental Figure S3 on the *Cell* website).

Finally, MBP-ERp44 interacted with GST-1L3V, but not with GST-2L3V or GST-3L3V (Figure 2K), which is consistent with the results of the initial screening with L3V-Fc and the IP experiment (Figures 1C and 1F, respectively). Based on all of the above findings, it was concluded that ERp44 directly interacts with the L3V domain of IP_3R1 in a subtype-specific and ER lumenal environment-dependent manner.

Expression of ERp44 Inhibits IICR via IP_3R1

To explore the functional consequences of ERp44 binding to IP_3R1, we performed Ca^{2+}-imaging experiments with the fluorescent Ca^{2+} indicator fura-2. First, we tested HeLa cells, approximately half of whose IP_3Rs are IP_3R1 (Hattori et al., 2004). Red fluorescent protein (RFP)-tagged ERp44 (RFP-ERp44) or RFP with an ER retention signal (RFP-RDEL, negative control) was then expressed in HeLa cells, and the cells were stimulated with ATP in Ca^{2+}-free medium. In nonexpressing cells, ATP (3 μM) typically caused a single Ca^{2+} transient, occasionally with small oscillations (Figure 3A, black trace), and the response of the cells expressing RFP-RDEL was indistinguishable from that of the nonexpressing cells (Figure 3A, red trace). Cells expressing RFP-ERp44, on the other hand, typically exhibited significantly smaller Ca^{2+} transients (Figure 3B, red trace), and the average peak amplitude in cells expressing RFP-ERp44 was significantly smaller (69.3% ± 1.8%, $p < 0.05$) than that in the nonexpressing cells (Figure 3C). The difference was not due to a decrease in releasable Ca^{2+} in the ER because the amount of the passive Ca^{2+} leakage elicited by Tg was unchanged (Figures 3D and 3E). Also, IP_3 production was not influenced by overexpression of ERp44 (data not shown).

Next, we tested the effect of ERp44 overexpression in COS-7 cells because they are known to express no IP_3R1 (Boehning and Joseph, 2000; Hattori et al., 2004). Stimulation of cells expressing RFP-RDEL with 1 μM ATP typically elicited a single Ca^{2+} transient (Figure 3F), while expression of RFP-ERp44 had no effect on the pattern or amplitude of the transient (Figures 3G and 3H). No effect of RFP-ERp44 expression was observed when cells were stimulated with lower ATP concentrations (0.3 μM) (data not shown).

The above results suggest that ERp44 inhibits IP_3R1 but does not inhibit IP_3R2 or IP_3R3. To further confirm this, we needed to compare cells that express IP_3R1 only to those expressing no IP_3R1. This was achieved by employing DT40-KMN60 and DT40-1KO cells, both of which were derived from the same parent cell line, DT40 cells. The DT40-KMN60 cell line was established by stably transfecting the mouse IP_3R1 gene on a background of IP_3R-deficient DT40 cells (DT40-TKO, Sugawara et al., 1997). DT40-1KO cells express IP_3R2 and IP_3R3, but not IP_3R1 (Sugawara et al., 1997). Crosslinking of the B cell antigen receptor (BCR) activates PLC-γ, which results in production of IP_3 in DT40 cells. The peak amplitude of BCR-induced Ca^{2+} release in DT40-KMN60 cells expressing RFP-RDEL was approximately the same (96% ± 2.9%) as in nonexpressing cells (Figure 3K), but it was significantly smaller in DT40-KMN60 cells expressing RFP-ERp44 (60.6% ± 9.6%, Figures 3I and 3K). There was no reduction in Tg-induced Ca^{2+} leakage

---

was cleaved by thrombin and the GST released then was removed by incubation with GSH-Sepharose. This ERp44 protein was incubated with GST-1L3V in neutral solution (pH 7.5) containing 5 mM EGTA in the presence or absence of 3 mM DTT. The inputs and bead bound proteins were resolved with SDS-PAGE under nonreducing conditions and analyzed by Western blotting with α-ERp44 (top and middle) or α-GST (bottom).

(D) Purified GST-1L3V (lane 1) and its cysteine mutants, C2496S (lane 2), C2504S (lane 3), C2527S (lane 4), and 3CS (C2496S/C2504S/C2527S, lane 5), were incubated with ERp44 (as prepared in [C]) in the presence of 3 mM DTT and 5 mM EGTA. Proteins were then precipitated with GSH-Sepharose and subjected to Western blotting with α-ERp44 (middle) or α-GST (bottom). The amount of ERp44 added to the binding reaction is shown at the top. The histogram depicts densitometric analyses from five independent experiments.

(E) Ca^{2+} dependency of the interaction between 1L3V with ERp44. A binding assay was performed with 3 mM DTT in the presence of EGTA or the Ca^{2+} concentration indicated. Proteins bound to GSH-Sepharose were subjected to Western blotting with α-MBP (top) or α-GST (bottom).

(F) In vivo interaction between IP_3R1 and ERp44 is enhanced under reducing conditions. COS-7 cells expressing GFP-IP_3R1 and HA-ERp44 were treated with 5 mM DTT for 30 min (+) or not (−), then treated with DSP, and IP was performed. The lysates and IP samples were analyzed by Western blotting with α-GFP (top and middle) or α-HA (bottom).

(G and H) In vivo interaction between IP_3R1 and ERp44 is enhanced after ER Ca^{2+} depletion. COS-7 cells expressing GFP-IP_3R1 and HA-ERp44 were stimulated with 10 μM ATP (+) or not (−) for 5 min (G), or 2 μM Tg (+) or not (−) for 30 min (H), treated with DSP, and finally IP was performed. The lysates and IP samples were analyzed by Western blotting with α-GFP or α-HA.

(I) Schematic representation of ERp44 and its mutants.

(J) Amino acid residues 236–285 of ERp44 are responsible for interaction with 1L3V. GST-1L3V was incubated with MBP (lane 1) or MBP fusion proteins containing subfragments of ERp44 (lanes 2–8). Binding assay was performed as in (E). The "control" MBP protein (lane 1) is in fact MBP plus 94 unrelated amino acids derived from the vector (pMAL-c) sequence and its molecular weight is thus larger than those of some ERp44-fusion proteins.

(K) ERp44 specifically interacts with the L3V of IP_3R1, but not that of IP_3R2 or IP_3R3. Purified GST (lane 1), GST-1L3V (lane 2), GST-2L3V (lane 3), or GST-3L3V (lane 4) was incubated with MBP-ERp44 in neutral solution (pH 7.5) containing EGTA and DTT. Proteins bound to GSH-Sepharose were subjected to Western blotting with α-MBP (top and middle) or α-GST (bottom).

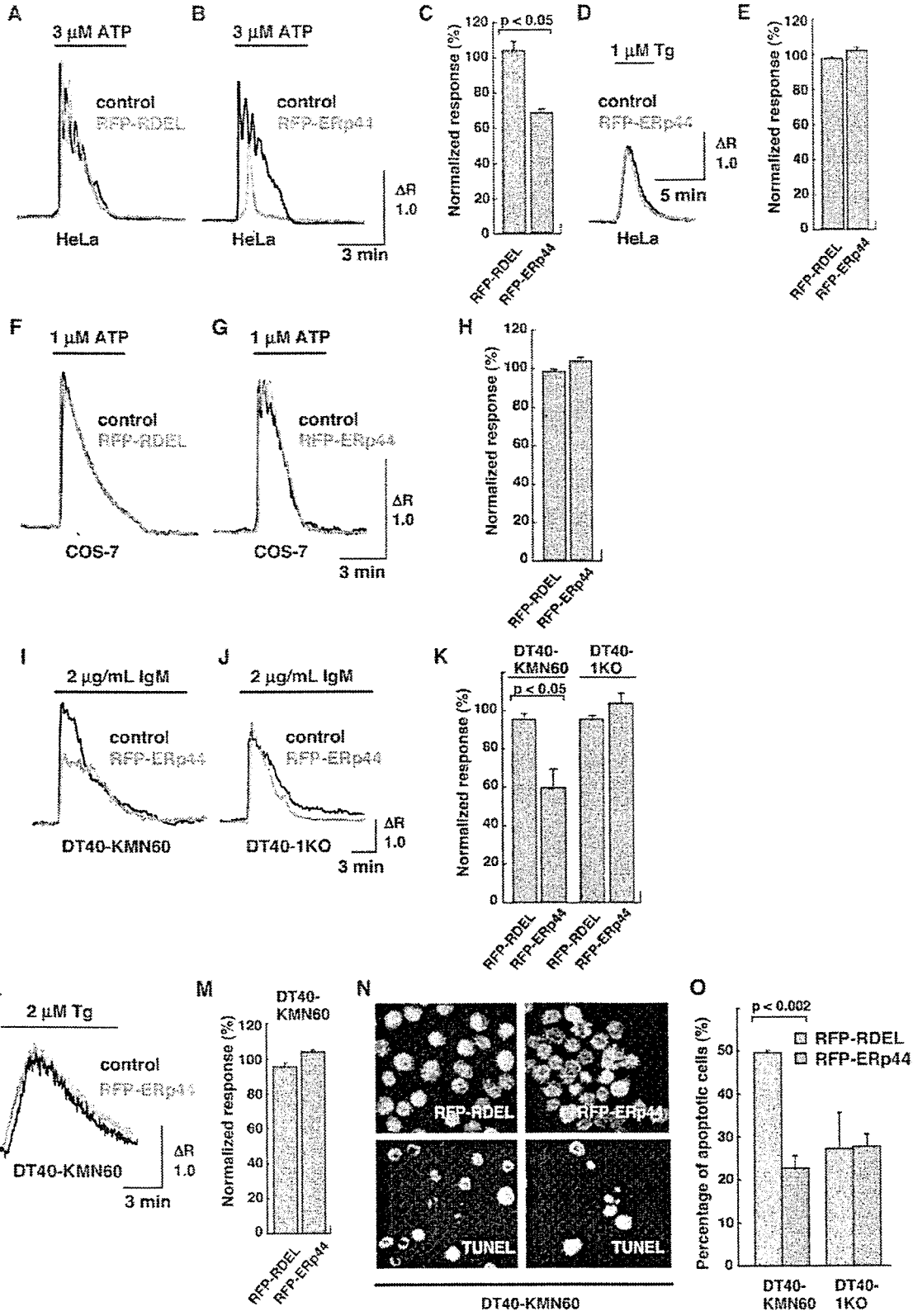
A
3 μM ATP
control
RFP-RDEL
HeLa
B
3 μM ATP
control
RFP-ERp44
HeLa
ΔR
1.0
3 min
C
p < 0.05
Normalized response (%)
RFP-RDEL
RFP-ERp44
D
1 μM Tg
control
RFP-ERp44
ΔR
1.0
5 min
HeLa
E
Normalized response (%)
RFP-RDEL
RFP-ERp44
F
1 μM ATP
control
RFP-RDEL
COS-7
G
1 μM ATP
control
RFP-ERp44
COS-7
ΔR
1.0
3 min
H
Normalized response (%)
RFP-RDEL
RFP-ERp44
I
2 μg/mL IgM
control
RFP-ERp44
DT40-KMN60
J
2 μg/mL IgM
control
RFP-ERp44
DT40-1KO
ΔR
1.0
3 min
K
DT40-KMN60
DT40-1KO
p < 0.05
Normalized response (%)
RFP-RDEL
RFP-ERp44
RFP-RDEL
RFP-ERp44
L
2 μM Tg
control
RFP-ERp44
DT40-KMN60
ΔR
1.0
3 min
M
DT40-KMN60
Normalized response (%)
RFP-RDEL
RFP-ERp44
N
RFP-RDEL
RFP-ERp44
TUNEL
TUNEL
DT40-KMN60
O
p < 0.002
RFP-RDEL
RFP-ERp44
Percentage of apoptotic cells (%)
DT40-KMN60
DT40-1KO

in these cells (Figures 3L and 3M). In DT40-1KO cells, on the other hand, expression of RFP-ERp44 had little effect on the peak amplitude (Figures 3J and 3K). These results indicate that ERp44 inhibits IP_3R1, but not IP_3R2 or IP_3R3.

IP_3Rs have a critical function in BCR-induced apoptosis in DT40 cells (Sugawara et al., 1997). We found that expression of REP-ERp44, but not RFP-RDEL, significantly inhibited apoptosis in DT40-KMN60 cells (Figures 3N and 3O), but no such effect was observed in DT40-1KO cells (Figure 3O), implying that inhibition of IP_3R1 by ERp44 affects cell functions, such as apoptosis.

Specific Knockdown of ERp44 Results in Augmentation of IICR via IP_3R1

Next, we used the RNA interference technique to investigate the role of endogenous ERp44 by testing two different small interfering RNA (siRNA) sequences targeted to the open reading frame (siERp44-ORF) and the 3′-untranslated region (siERp44-3U), respectively, of human ERp44. To provide negative controls, we introduced three-point mutations in these siRNAs (siControl-ORF or siControl-3U, respectively). Western analysis revealed both siERp44-ORF and siERp44-3U to efficiently and specifically "knock down" ERp44 in HeLa and COS-7 cells (Figure 4A). Unfortunately, however, none of the siRNAs targeted to chicken ERp44 decreased the amount of ERp44 in DT40 cells (data not shown). In HeLa cells, knockdown of ERp44 neither affected the expression of other ER oxidoreductases nor induced unfolded protein response within 48 hr (Supplemental Figure S5 online).

SiRNA-transfected HeLa cells were stimulated with 1, 3, and 10 μM ATP. Stimulation with 1 μM ATP rarely (4.0% ± 0.3% of all cells) evoked discernible Ca^{2+} signals in siControl-3U-transfected cells (Figures 4B and 4C, black trace and bar), whereas approximately five times the number (20.1% ± 2.5%) of siERp44-3U-transfected cells responded (Figures 4B and 4C, red trace and bar). Subsequent stimulation with 3 μM ATP elicited IICR in 46.9% ± 1.6% of the control cells and 90.3% ± 1.2% of the cells transfected with siERp44-3U (Figures 4B and 4C), whereas most of the cells in both preparations responded when stimulated with 10 μM ATP (Figure 4C). The average peak amplitude was higher in siERp44-3U-transfected cells than in the siControl-3U-transfected cells at all ATP concentrations (Figure 4D). These ERp44 knockdown effects were confirmed to be specific by transfecting the cells with RFP-ERp44 ("rescue" experiments, Supplemental Figure S4). Knockdown of ERp44 had no effect on the Ca^{2+} leakage induced by Tg (data not shown).

We then performed the same experiments in COS-7 cells. Since COS-7 cells do not express IP_3R1, we predicted that knockdown of ERp44 would have no effect on IICR in this cell line, and the results confirmed our prediction (Figures 4E–4G). These findings indicate that ERp44 specifically inhibits IP_3R1.

Cysteine Residues in the L3V Domain Are Important for Inhibition of IP_3R1 Activity by ERp44

Next, we investigated the significance of the cysteine residue(s) in 1L3V in terms of the inhibition of IP_3R1 by ERp44. We first investigated whether mutations of these residues in full-length (and GFP-tagged) IP_3R1 affected IICR activity (Figure 5A). When Cys2527, which is located adjacent to the channel pore region, was mutated, channel activity was completely lost (Figure 5A), and this mutant was not used any further. Mutations in Cys2496 and Cys2504, however, had no effect on channel activity (Figure 5A). Interaction between these IP_3R1 mutants and ERp44 was significantly decreased (Figure 5B), consistent with the results obtained with recombinant proteins (Figure 2D). The IP_3R1 mutant was cotransfected into DT40-TKO cells with either RFP-RDEL or RFP-ERp44, and a Ca^{2+}-imaging experiment was performed. IICR via GFP-IP_3R1 (i.e., wild-type) was suppressed by coexpression with RFP-ERp44, but not with RFP-RDEL (Figures 5C and 5F). Surprisingly, this inhibition by ERp44 was almost completely abolished by substitution of the Cys2496 or Cys2504 of GFP-IP_3R1 (Figures 5D and 5E, respectively, and Figure 5F). These results clearly demonstrated that the presence of free thiol groups in the L3V domain is important for inhibition of IP_3R1 by ERp44.

ERp44 Inactivates Channel Activity of IP_3R1 in Lipid-Bilayer System

To unambiguously demonstrate that ERp44 inhibits IP_3R1, we performed single-channel current recording

Figure 3. Expression of ERp44 Inhibits IICR in HeLa and DT40-KMN60 Cells, but Not in COS-7 or DT40-1KO Cells

(A and B) ERp44 inhibits IICR in HeLa cells. Cells transfected with either RFP-RDEL (A) or RFP-ERp44 (B) were stimulated with 3 μM ATP. Representative Ca^{2+} responses in nonexpressing (black) and expressing cells (red) are shown.

(C) Quantitation of results in (A) and (B). Normalized responses were calculated with the averaged peak amplitude of nonexpressing cells set equal to 100%. $p < 0.05$ compared to RFP-RDEL (Student's t test).

(D) The Ca^{2+} storage capacity is unchanged in HeLa cells expressing RFP-ERp44. Cells were stimulated with 1 μM Tg, and representative Ca^{2+} responses in nonexpressing (black) and expressing cells (red) are shown.

(E) Quantitation of the results in (D).

(F–H) ERp44 does not affect IICR in COS-7 cells. Cells transfected with either RFP-RDEL (F) or RFP-ERp44 (G) were stimulated with 1 μM ATP. Representative Ca^{2+} responses in nonexpressing (black) and expressing cells (red) are shown.

(H) Quantitation of results shown in (F) and (G).

(I–K) ERp44 inhibits IICR in DT40-KMN60 but not in DT40-1KO cells. Cells were stimulated with 2 μg/ml anti-IgM. Representative Ca^{2+} responses in nonexpressing (black) and expressing cells (red) are shown, and their quantitations are shown in (K).

(L and M) ERp44 does not affect Ca^{2+} storage capacity in DT40-KMN60 cells. Ca^{2+} responses in nonexpressing (black) and expressing cells (red) and their quantitations are shown in (M).

(N and O) ERp44 inhibits BCR-induced apoptosis in DT40-KMN60 cells, but not in DT40-1KO cells. Cells were treated with anti-IgM (2 μg/ml) for 24 hr and apoptosis was assessed by TUNEL assay. Data are TUNEL-positive cells as a percentage of all cells expressing RFP-RDEL (gray) or RFP-ERp44 (red) from two independent experiments. $p < 0.002$ compared with RFP-RDEL (Student's t test).

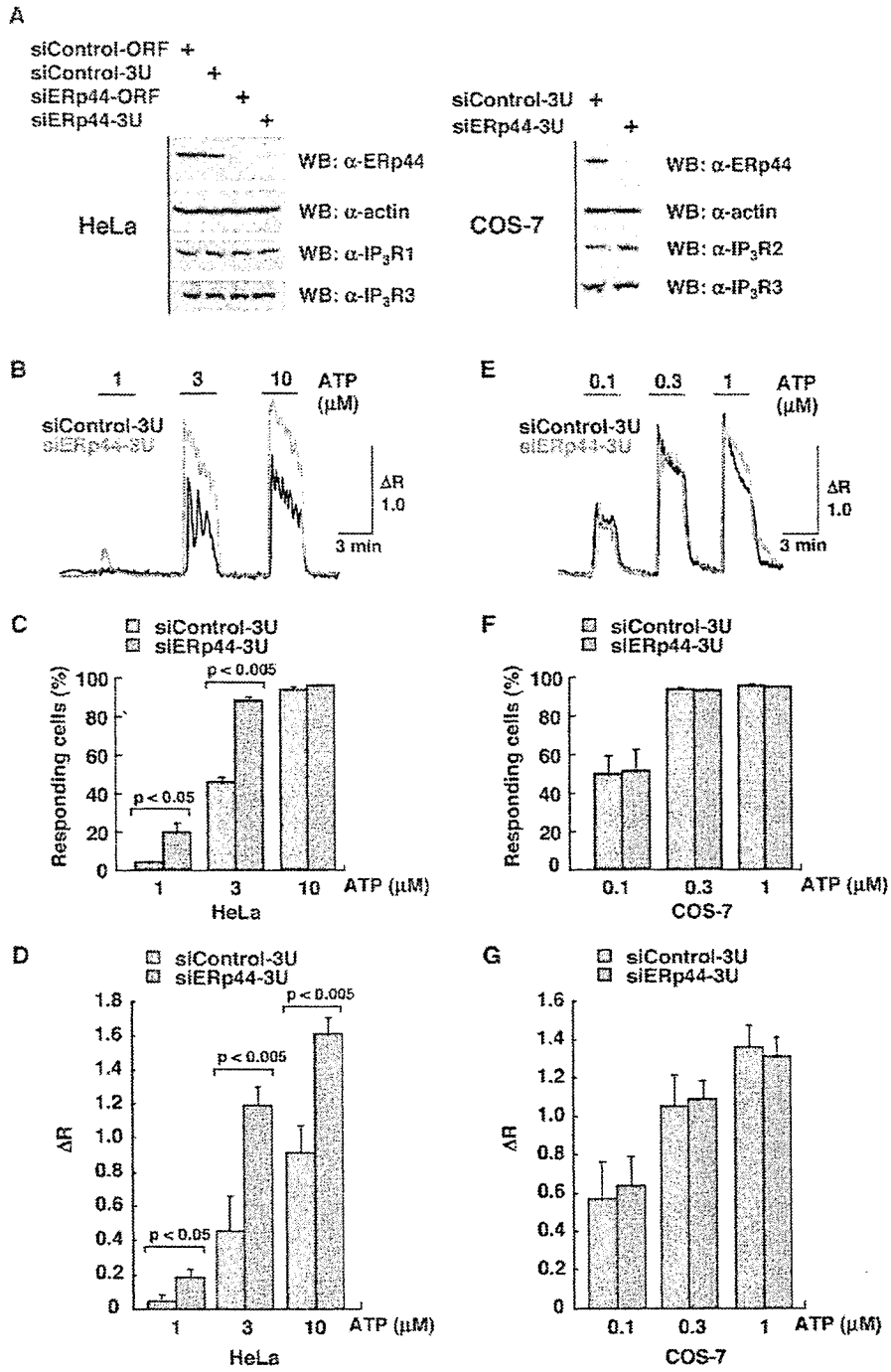

Figure 4. Knockdown of ERp44 Augments IICR in HeLa Cells, but Not in COS-7 Cells

(A) Knockdown of ERp44 in HeLa and COS-7 cells. The lysates of HeLa (left) and COS-7 cells (right) transfected with the siRNA indicated were analyzed by Western blotting with the antibodies indicated.

(B) Knockdown of ERp44 augments IICR in HeLa cells. Cells were stimulated with 1, 3, and 10 μM ATP in the presence of extracellular Ca^{2+}. Representative Ca^{2+} responses in siControl-3U-transfected (black) or siERp44-3U-transfected cells (red) are shown.

(C) Percentages of HeLa cells transfected with siControl-3U (gray) or siERp44-3U (red) that showed discernible Ca^{2+} responses at the ATP concentrations indicated.

(D) Average peak amplitude of the Ca^{2+} response in HeLa cells transfected with siControl-3U (gray) or siERp44-3U (red).

(E) COS-7 cells were stimulated with 0.1, 0.3, and 1 μM ATP in the presence of extracellular Ca^{2+}. Representative Ca^{2+} responses in siControl-3U-transfected (black) and siERp44-3U-transfected cells (red) are shown.

(F) Percentages of COS-7 cells transfected with siControl-3U (gray bars) or siERp44-3U (red bars) that showed discernible Ca^{2+} responses at the ATP concentrations indicated.

(G) Average peak amplitude of the Ca^{2+} response in COS-7 cells transfected with siControl-3U (gray columns) or siERp44-3U (red columns).

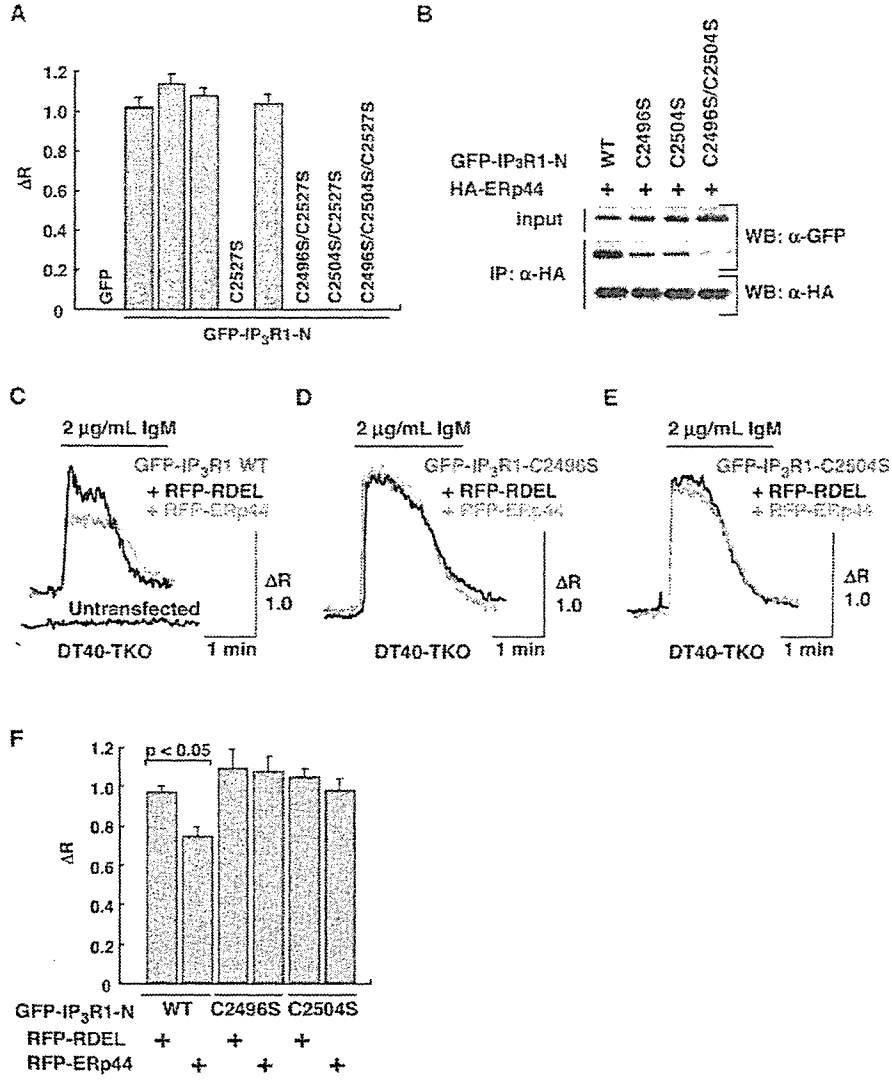

Figure 5. Cysteine Residues of 1L3V Are Required for Inhibition of IP_3R1 by ERp44

(A) DT40-TKO cells expressing GFP, GFP-IP_3R1, or GFP-IP_3R1 with cysteine replacements were stimulated with 2 μg/ml anti-IgM. Average peak amplitudes of the Ca^{2+} response are shown.

(B) Cysteine residues of the L3V domain of IP_3R1 are important for interaction between IP_3R1 and ERp44. GFP-IP_3R1 or its cysteine mutant was transfected with HA-ERp44 in COS-7 cells. Thirty-six hours after transfection, the cells were treated with DSP, and IP was performed with anti-HA. The lysates and IP samples were analyzed by Western blotting with α-GFP (top and middle) or α-HA (bottom).

(C–E) ERp44 inhibits IICR in DT40-TKO cells expressing IP_3R1, but not in cells expressing IP_3R1 cysteine mutants. RFP-RDEL or RFP-ERp44 was transfected into DT40-TKO cells with GFP-IP_3R1 or its cysteine mutant. Thirty-six hours after transfection, the cells were stimulated with 2 μg/ml anti-IgM. Representative Ca^{2+} responses in RFP-RDEL-expressing (black) and RFP-ERp44-expressing cells (red) are shown.

(F) Summary of the Ca^{2+}-imaging experiments in (C)–(E). Average peak amplitudes of the ratios are shown.

in a planar lipid bilayer fused with mouse cerebellar microsomes in which 99% of the IP_3Rs are IP_3R1 (Taylor et al., 1999). We first confirmed the interaction between MBP-ERp44 and GST-1L3V in the lumenal-side solution containing 3 mM DTT (Figure 6A). IP_3R1 activity was recorded with Ba^{2+} as a charge carrier in the presence of 3 mM DTT in the trans (lumenal) compartment. Addition of MBP-ERp44 resulted in inhibition of the channel activity in a dose-dependent manner (Figures 6B–6E), but addition of MBP (negative control) to the lumenal compartment had no effect on IP_3R1 activity (data not shown). Whether or not addition of more MBP-ERp44 can completely block the channel activity was not testable since we were unable to obtain a more concentrated recombinant ERp44 protein and adding more of the solution had nonspecific effects on channel activity (data not shown). ERp44 decreased the frequency of channel opening, but did not affect the mean open time of the channel (1.6 ± 0.5 ms and 1.5 ± 0.7 ms [mean ± SD, n = 6] before and after addition of 7.5 μM MBP-ERp44,